Phenotyping and auto-antibody production by liver-infiltrating B cells in primary sclerosing cholangitis and primary biliary cholangitis

Chung, Brian; Guevel, Bardia T.; Reynolds, Gary; Gupta Udatha, D.B.R.K.; Henriksen, Eva Kristine Klemsdal; Stamataki, Zania; Hirschfield, Gideon; Karlsen, Tom Hemming; Liaskou, Evaggelia

DOI:
10.1016/j.jaut.2016.10.003

Phenotyping and auto-antibody production by liver-infiltrating B cells in primary sclerosing cholangitis and primary biliary cholangitis

Brian K. Chung,[1,2,3] Bardia T. Guevel,[1] Gary M. Reynolds,[1] D.B.R.K Gupta Udatha,[2,4,5] Eva Kristine Klemsdal Henriksen,[2,3,4,5] Zania Stamataki,[1] Gideon M. Hirschfield,[1]* Tom Hemming Karlsen,[2,3,4,5]* and Evaggelia Liaskou[1]

[1] Centre for Liver Research and NIHR Birmingham Liver Biomedical Research Unit, Institute of Immunology and Immunotherapy, University of Birmingham, Birmingham, UK

[2] Norwegian PSC Research Center, Department of Transplantation Medicine, Division of Surgery, Inflammatory Medicine and Transplantation, Oslo University Hospital Rikshospitalet, Oslo, Norway

[3] Institute of Clinical Medicine, Faculty of Medicine, University of Oslo, Oslo, Norway

[4] Research Institute of Internal Medicine, Division of Surgery, Inflammatory Medicine and Transplantation, Oslo University Hospital Rikshospitalet, Oslo, Norway

[5] K.G. Jebsen Inflammation Research Centre, Institute of Clinical Medicine, University of Oslo, Oslo, Norway

* Indicates corresponding authors

Keywords

primary biliary cholangitis, primary sclerosing cholangitis, antibody-secreting B cells, autoimmunity, auto-antibodies, protein arrays, biomarkers

Corresponding Authors

*Prof G M Hirschfield, Centre for Liver Research, NIHR Birmingham Liver Biomedical Research Unit, Institute of Immunology and Immunotherapy, University of Birmingham, Birmingham, UK, B15 2TT.

Email: g.hirschfield@bham.ac.uk

or

*Prof TH Karlsen, Norwegian PSC Research Center, Department of Transplantation Medicine, Division of Surgery, Inflammatory Medicine and Transplantation, Oslo University Hospital Rikshospitalet, Postboks 4950 Nydalen, N-0424 Oslo, Norway.

Email: t.h.karlsen@medisin.uio.no

List of Abbreviations

primary biliary cholangitis (PBC), primary sclerosing cholangitis (PSC), human leukocyte antigen (HLA), anti-mitochondrial antibodies (AMA), antibody-secreting B cells (ASCs), liver-infiltrating mononuclear cells (LIMCs), anti-nuclear antibodies (ANA), kelch-like 12 (KLHL12), hexokinase 1 (HK1), perinuclear anti-neutrophil cytoplasmic antibodies (pANCA), celiac disease (CD), type 1 diabetes (T1D), nucleolar protein 3 (NOL3), immunofluorescence (IF), immunoblotting (IB), hematopoietic cell-specific Lyn substrate 1 (HCLS1), adhesion G protein-coupled receptor A3 (ADGRA3), ATPase type 13A5 (ATP13A5), integrin beta-like 1 (ITGBL1), potassium channel tetramerization domain containing 13 (KCTD13), keratin associated protein 5-4 (KRTAP5-4), PRAME family member 12 (PRAMEF12), proline-rich coiled-coil 2B (PRRC2B), serine/arginine-rich splicing factor 1 (SFRS1), TEA domain family member 3 (TEAD3), phosphatase 1 regulatory subunit 11 (PP1R11), endothelin converting enzyme 2 (ECE2), inflammatory bowel disease (IBD), T cell receptor (TCR), β-tubulin isotype 5 (TBB-5)

Highlights

- Disease restricted auto-antibody signatures can potentially inform disease pathophysiology
- Liver-infiltrating antibody-secreting B cells (ASCs) are reduced in PSC compared to PBC
- Cultured liver-infiltrating ASCs in PSC and PBC produce auto-antibodies
- Liver-infiltrating ASCs in PBC secrete auto-antibodies to HK1 and PDC-E2
- Auto-antibodies from liver-infiltrating ASCs in PSC share reactivity to novel antigen targets

Abstract

Primary biliary cholangitis (PBC) and primary sclerosing cholangitis (PSC) are immune-mediated biliary diseases that demonstrate prominent and restricted genetic association with human leukocyte antigen (HLA) alleles. In PBC, anti-mitochondrial antibodies (AMA) are specific and used as diagnostic biomarkers. PSC-relevant auto-antibodies remain controversial despite a distinct HLA association that mirrors archetypical auto-antigen driven disorders. Herein, we compared antibody-secreting B cells (ASCs) in PSC and PBC liver explants to determine if liver-infiltrating ASCs represent an opportune and novel source of disease-relevant auto-antibodies. Using enzymatic digestion and mechanical disruption, liver mononuclear cells (LIMCs) were isolated from fresh PSC and PBC explants and plasmablast ($CD19+CD27+CD38^{hi}CD138-$) and plasma cell ($CD19+CD27+CD38^{hi}CD138+$) ASCs were enumerated by flow cytometry. We observed 45-fold fewer plasma cells in PSC explants ($n = 9$) compared to PBC samples ($n = 5$, $p < 0.01$) and 10-fold fewer IgA-, IgG- and IgM-positive ASCs ($p < 0.05$). Liver-infiltrating ASCs from PSC and PBC explants were functional and produced similar concentrations of IgA, IgG and IgM following 2 weeks of culture. Antibody production by PBC ASCs ($n = 3$) was disease-specific as AMA to pyruvate dehydrogenase complex E2 subunit (PDC-E2) was detected by immunostaining, immunoblotting and ELISA. Antibody profiling of PSC supernatants ($n = 9$) using full-length recombinant human protein arrays (Cambridge Protein Arrays) revealed reactivities to nucleolar protein 3 (5 / 9) and hematopoietic cell-specific Lyn substrate 1 (3 / 9). Array analysis of PBC supernatants ($n = 3$) detected reactivities to PDC-E2 and hexokinase 1 (3 / 3). In conclusion, we detected unique frequencies of liver-infiltrating ASCs in PSC and PBC and in so doing, highlight a feasible approach for understanding disease-relevant antibodies in PSC.

1. Introduction

Primary biliary cholangitis (formerly known as cirrhosis; PBC) and primary sclerosing cholangitis (PSC) are immune-mediated cholestatic liver diseases of unknown etiology. PBC is prototypically autoimmune with a characteristic serologic profile: anti-mitochondrial antibodies (AMA) to the E2 subunit of pyruvate dehydrogenase complex (PDC-E2) and anti-nuclear antibodies (ANA) to gp210 and sp100 are sensitive and specific diagnostic biomarkers. Other PBC-specific auto-antibody targets include kelch-like 12 (KLHL12) and hexokinase 1 (HK1) [1,2]. Although PBC and PSC are characterized by chronic inflammatory insults to the biliary tree with subsequent cholestasis and progressive biliary fibrosis, the nature and site of biliary inflammation are distinct.

One area in which our understanding of the underlying disease biology has advanced significantly has been through genetic risk association studies [3]. For PBC and PSC, significant HLA and non-HLA genetic associations are evident, and whilst in essence are non-overlapping, confirm dominant HLA associations for both diseases [4,5]. In the case of PBC, such HLA associations have been used to understand the role of PDC-E2 in disease pathogenesis as patients who are anti-sp100 seropositive have distinct HLA profiles [6]. Similar findings relating to anti-cyclic citrullinated antibodies have also been observed in rheumatoid arthritis (RA) [7]. In the setting of PSC, characteristic auto-antibodies remain to be demonstrated. There are diverse reports of auto-antibodies to biliary and colonic epithelial antigens, neutrophil granulocytes (perinuclear anti-neutrophil cytoplasmic antibodies; pANCA) and several ubiquitous self-antigens however all of these are lacking robust validation and/or disease specificity [8]. This is an anomaly given the nature and strength of the genetic HLA association seen in PSC [9,10]

which strongly resembles archetypical autoimmune disorders such as celiac disease (CD) and type 1 diabetes (T1D) [11].

Previous studies assessing liver-infiltrating ASCs from PSC and PBC patients are inconclusive [12,13] and our general understanding of antibody-secreting B cells (ASCs) within the liver is limited. For example, it is unknown if the main constituents of the ASC population, namely short-lived plasmablasts and long-lived plasma cells, are present in unique frequencies in PSC and PBC liver. Such distinctions could be important for the treatment of PSC as auto-antibody production in PBC patients was significantly reduced upon selective plasmablast depletion using anti-CD20 monoclonal antibody (rituximab) [14]. Recent evidence in RA also suggests that plasmablasts at sites of active inflammation may act as the primary source of disease-relevant auto-antibodies [15,16]. Hence, differences in the relative proportions and absolute numbers of liver-infiltrating plasmablasts and plasma cells in PSC and PBC may influence disease-relevant auto-antibody concentrations.

By inference to the HLA risk association studies in PSC, we therefore hypothesize that PSC has triggers that include a distinct repertoire of antigenic targets and associated auto-antibodies that are disease-specific, and potentially are more readily identified from liver. Herein we report the isolation of fresh PSC and PBC liver-infiltrating mononuclear cells (LIMCs) to characterize the plasmablast and plasma cell ASC subsets, to confirm the production of disease-relevant auto-antibodies by PBC ASCs and to capture the auto-antibody profile of PSC ASCs using recombinant human protein arrays, with AMA in PBC as a methodologic control.

2. Methods and Materials

2.1. Human liver tissue and study cohort.

Fresh PSC and PBC liver explants were collected through the transplantation program at Queen Elizabeth Hospital in Birmingham, United Kingdom and were obtained with patient consent and in accordance with local research ethics committee approval (LREC #06-Q2702-61). Clinical details of the PSC and PBC study cohorts are listed in Table 1. Sample numbers (n) for each experiment are provided within the figure legends.

2.2. Isolation of liver-infiltrating mononuclear cells (LIMCs) and enrichment for ASCs.

PSC and PBC liver sections were cut into 1-2 mm^3 pieces, thoroughly washed 3-4 times with PBS and resuspended in digestion media [RPMI 1640, 3% FBS, collagenase type 1A (VWR International)] at 37º C for 30 min. Digested tissue was mechanically homogenized using a Stomacher400 circulator (Seward) and washed repeatedly with PBS through 63 μm nylon filters. Washed tissue was discarded and the filtered cell suspension was aliquoted into 50 ml conical tubes and spun at 600 g for 5 min. Supernatant was discarded and cell pellets were resuspended and washed 3-4 times with PBS. Following the final wash, cell pellets were resuspended in PBS and LIMCs were isolated by density centrifugation using Lympholyte-H (Cedarlane). Collected LIMCs were resuspended in PBS and the total cells per gram of tissue was calculated using a hemocytometer (Hawksley).

2.3. Antibodies and flow cytometry.

LIMCs transferred to 96-well U-bottom plates (1 x 10^6 cells/well) were stained with anti-human CD3 FITC (BD Pharmingen; clone HIT3a), CD19 PE-eFluor610 (Biolegend; clone HIB19),

CD27 Brilliant Violet510 (Biolegend; clone LG.3A10), CD38 PE (eBiosciences; clone HB7), CD138 APC (eBioscience; clone DL-101), IgM eFluor450 (eBioscience; clone SA-DA4), IgG PerCP/Cy5.5 (Biolegend; clone M1310G05), IgA PE-Vio770 (Miltenyi Biotec; clone IS11-8E10) and Zombie NIR viability dye (Biolegend). Data was acquired using a CyAn 9-colour flow cytometer (Beckman Coulter) and analyzed by FlowJo 8.7 (Treestar).

2.4. Immunohistochemistry for CD20 and NOL3.

Formalin-fixed paraffin-embedded PSC and PBC liver tissue was dewaxed and rehydrated with water after low temperature retrieval [17]. Sections were immunostained with anti-human CD20 (ImPath; clone L26) or nucleolar protein 3 (NOL3, Sigma-Aldrich; clone ABC837), counterstained with haematoxylin and mounted with a glass coverslip. Tissue slides were scanned (ZxioScan.Z1, Zeiss) and CD20 staining was quantified by Image Processing and Analysis in Java (ImageJ, NIH) using a single colour threshold analysis of 10 representative areas of B cell infiltration near portal tracts and bile ducts. Magnification, dimensions and colour thresholds for each representative image area were kept identical between samples. NOL3 staining intensity was graded as negative (–), weak (+), moderate (++) and strong (+++). Muscle present in the vasculature served as an internal positive control showing moderate cytoplasmic and strong nuclear staining. IgG controls were negative (Supplementary Figure 1).

2.5. LIMC culture and IgA, IgG, IgM ELISA.

Freshly isolated LIMCs were resuspended in culture media (RPMI 1640, 10% FBS, L-glutamine, 1X penicillin-streptomycin) and transferred to 24-well tissue culture plates (2 x 10^6 cells / ml; 1 ml total / well) and cultured in a humidified 37º C, 5% CO_2 incubator. Supernatant was harvested

at the indicated time points and stored at −80º C for batch analysis. Supernatant IgA, IgG and IgM were measured by ELISA. X50 Immulon 2HB 96-well flat-bottom plates (Fisher Scientific) were coated with LIMC culture supernatants overnight and serial dilutions of purified IgA (Sigma I1010), IgG (Sigma I4506) and IgM (Sigma I8260) were used as protein standards. IgA, IgG and IgM was detected using primary anti-human IgA (Dako; clone F0204), IgG (University of Birmingham; clone AF6) or IgM (University of Birmingham; clone R10) followed by anti-mouse or anti-rabbit HRP antibody staining (Jackson Laboratories; 715-035-151 and 111-035-003). HRP chromogenic substrate (SurModics) was added to each well followed by stop reagent (SurModics). Absorbance values at 450 nm and 550 nm were measured using a 96-well plate reader (Bio-TEK) and final absorbance values were calculated by subtracting 450 nm and 550 nm readings. All standards and samples were run in triplicate.

2.6. Indirect immunofluorescence, immunoblotting and ELISA for AMA.

PBC LIMC culture supernatants (day 14) were concentrated 20-fold by volume using 100K nominal molecular weight limit centrifugal filters (Millipore) [18] and tested for AMA using indirect immunofluorescence (IF), immunoblotting (IB) and ELISA. For IF staining, concentrated supernatants were incubated with rat stomach, liver and kidney tissue slides (NOVA Lite, Inova Diagnostics) for 20 mins at room temperature. Slides were washed with PBS, stained with fluorescent conjugate, washed again with PBS and mounted. Slides were viewed at 20X magnification using a fluorescence microscope (Axioskop 40, Zeiss) and imaged using AxioVision SE64 Rel. 4.9 software (Zeiss). For IB, concentrated supernatants were loaded manually onto immunoblot test strips (BlueDiver Dot LI7DIV-24, D-tek) and processed automatically on a BlueDiver instrument (D-tek). Dried strips were visually inspected for staining and imaged using a Photosmart C4480 scanner (Hewlett-Packard). For AMA ELISAs,

AMA concentrations were measured in concentrated PBC supernatants using anti-M2-3E ELISA kits (EA 1622-9601 G, Euroimmun) and relative units (RU) were calculated using a negative control.

2.7 High-density human recombinant protein microarrays.

Auto-antibody specificities of cultured LIMC supernatants were profiled using HuProt v1 and v2 protein arrays (Cambridge Protein Arrays). Briefly, recombinant human GST-tagged proteins were purified from yeast and printed on glass slides in duplicate. Slides were probed with LIMC culture supernatant (sample), biotinylated anti-GST antibody (positive control) or fresh culture media (negative control). Slides were washed and stained with fluorochrome-labeled anti-human IgA, IgG, IgM or streptavidin. Fluorescence intensities were measured by a plate photometer and analyzed by Scanarray Express software (PerkinElmer Life Sciences).

For each protein, the Z-score and Interaction Score (IS) were used to determine signals of significance or "hits" (Supplementary Figure 2). Z-scores represent the signal of a specific protein relative to the signal from a negative control protein and is calculated as: Z-score = $(F_{protein} - F_{average})$ / SD, where $F_{protein}$ = sample fluorescence of a specific protein minus fluorescence of negative control protein, $F_{average}$ = mean fluorescence of total protein array excluding control spots and SD = standard deviation. IS is the signal relative to the staining intensity of the same protein using anti-GST antibody and is calculated as: IS = $(HS / F_{GST\text{-}protein}) \times 10^3$, where $F_{GST\text{-}protein}$ = fluorescence intensity of a specific protein using the anti-GST antibody. Hits were defined as protein targets with a Z-score ≥ 1.5, an IS ≥ 0.3, a signal-to-noise ratio

(S/N) > 2.5 and a SD between duplicates < 0.25. All hits adhering to the above criteria were verified by visual inspection.

2.8. Statistical Analyses and Venn Diagram.

Statistical analyses were performed using Prism 6 (GraphPad). Data was tested for normality using the D'Agostino-Pearson omnibus test and statistical significance of non-parametric data was calculated using an unpaired two-way Mann-Whitney. Error bars represent the interquartile range and were calculated as the difference between the first and third quartiles. Statistical differences of $p < 0.05$ were considered significant. Venny 2.1 (Centro Nacional de Biotechnologia) was used to generate the Venn diagram depicting shared auto-antibody protein targets in PSC and PBC samples (Figure 6B).

3. Results

3.1. Frequencies and total numbers of liver-infiltrating B cells are decreased in PSC.

To determine if distinct frequencies or numbers of liver-infiltrating ASCs were present in PSC and PBC, we quantified the overall B cell population in fresh liver explants by immunohistochemistry (Figure 1A). Using CD20 as a general marker of B cell infiltration [19], we detected significantly fewer CD20+ cells surrounding the portal tracts and bile ducts in PSC compared to PBC (PSC: 1.05 ± 0.18%, PBC: 4.09 ± 1.5%; median ± standard error of mean; $p < 0.01$; Figure 1B). To confirm that total number of liver B cells were lower in PSC, we isolated LIMCs from fresh PSC and PBC explants using a combination of enzymatic digestion and mechanical digestion and enumerated the total B cell population (CD3–CD19+) by flow cytometry (Figure 1C). Consistent with our histology staining, we detected a 2.1-fold lower frequency of B cells within the total LIMC compartment of PSC patients (PSC: 9.9 ± 2.8%, PBC: 20.8 ± 7.0%, $p < 0.05$; Figure 1D) and 11-fold fewer B cells per gram of PSC liver tissue (PSC: 11,670 ± 3,428, PBC: 131,100 ± 40,460, $p < 0.05$; Figure 1E). Absolute numbers of LIMCs among PSC explants were also lower compared to PBC samples (PSC: $5.8 \times 10^5 \pm 1.5 \times 10^5$, PBC: $9.2 \times 10^5 \pm 4.4 \times 10^5$; Supplementary Figure 3).

3.2. PSC explants express lower numbers of liver-infiltrating plasma cells.

Next, we stained PSC and PBC LIMCs with anti-human CD19, CD27, CD38 and CD138 and evaluated the proportion and total number of liver-infiltrating ASCs [20-22]. No significant differences in the overall proportion of ASCs (CD19+CD27+$CD38^{hi}$) within the total B cell compartment of PSC and PBC samples was detected (Supplementary Figure 4) and we proceeded to divide ASCs into plasmablast (CD19+CD27+$CD38^{hi}$CD138–) and plasma cell

(CD19+CD27+CD38^{hi}CD138+) subsets using CD138 expression (Figure 2A). We observed that the majority of liver-infiltrating ASCs in PSC were plasmablasts (85.8 ± 4.9%) whereas PBC explants contained a significantly higher frequency of plasma cells (63.0 ± 5.9%, $p < 0.05$; Figure 2B) and absolute numbers of plasma cells per gram of liver tissue (PSC: 27 ± 18 cells, PBC: 1,227 ± 793 cells, $p < 0.01$; Figure 2C).

3.3. Liver-infiltrating IgM-positive plasma cells are lower in PSC than PBC.

To further characterize liver-infiltrating ASCs in PSC and PBC, plasmablasts and plasma cells were divided into IgA-positive, IgM-positive and IgG-positive subsets based on surface staining (Figure 3A) as intracellular staining of IgA, IgM and IgG identified a similar frequency of ASCs compared to surface staining alone (Supplementary Figure 5). In PSC, we detected a higher frequency of IgA-positive plasmablasts (PSC: 13.3 ± 3.6%, PBC: 3.1% ± 7.2%) and IgG-positive plasmablasts (PSC: 22.8 ± 5.6%, PBC: 11.3 ± 5.6%) and lower proportions of IgM-positive plasmablasts (PSC: 5.0 ± 2.5%, PBC: 9.6 ± 4.4%) compared to PBC (Figure 3B). PSC and PBC explants contained similar frequencies of IgA-positive plasma cells (PSC: 8.1 ± 2.5%, PBC: 10.2 ± 5.4%) and IgG-positive plasma cells (PSC: 19.4 ± 4.2, PBC: 21.0 ± 4.7%) however PSC samples contained a significantly lower proportion of IgM-positive plasma cells compared to PBC (PSC: 5.6 ± 1.5%, PBC: 17.6 ± 6.3%, $p < 0.01$; Figure 3B). In terms of absolute numbers, we observed slightly fewer IgA-positive and IgG-positive plasmablasts and significantly fewer IgM-positive plasmablasts and plasma cells in PSC explants compared to PBC (Figure 3C). IgA-positive plasmablasts (PSC: 26 ± 35 cells, PBC: 80 ± 50 cells) and IgA-positive plasma cells (PSC: 6 ± 2 cells, PBC: 92 ± 315 cells, $p < 0.05$) per gram of liver tissue were rare in PSC and PBC relative to the number of IgG-positive and IgM-positive plasmablasts (IgG-positive PSC: 168 ± 63 cells, PBC: 552 ± 265 cells; IgM-positive PSC: 28 ± 16 cells, PBC: 648 ± 229 cells, $p <$

0.05) and IgG-positive and IgM-positive plasma cells (IgG-positive PSC: 37 ± 29 cells, PBC: 833 ± 259 cells; IgM-positive PSC: 4 ± 9 cells, PBC: 476 ± 556 cells, $p < 0.05$).

3.4. LIMCs enriched from PSC and PBC explants contain functional ASCs.

To determine if liver-infiltrating ASCs from end-stage PSC and PBC patients were functional, LIMCs from fresh explants were cultured and IgA, IgG and IgM supernatant concentrations were quantified by ELISA. After 1 day in culture, PSC and PBC ASCs from liver produced modest concentrations of antibody that continued to accumulate in supernatant for 2 weeks (Figure 4A). At day 14, similar concentrations of IgA (PSC: 2.5 ± 1.5 μg/ml, PBC: 2.8 ± 1.7 μg/ml), IgG (PSC: 3.8 ± 0.8 μg/ml, PBC: 2.5 ± 1.2 μg/ml) and IgM (PSC: 2.7 ± 1.0 μg/ml, PBC: 2.7 ± 1.3 μg/ml) were measured in PSC and PBC supernatants (Figure 4B). We noted that liver-infiltrating ASCs from 2 PSC patients produced significantly higher levels of IgA at day 14 compared to the average PSC cohort (high IgA samples: 22.8 ± 0.2 μg/ml, average IgA samples: 2.2 ± 0.8 μg/ml; $p < 0.01$, Supplementary Figure 6). The significance of this observation is undetermined as antibody concentrations in LIMC cultures did not directly correlate with paired IgA, IgG and IgM serum titres measured at earlier time points (Supplementary Figure 7).

3.5. Culture supernatant from liver-infiltrating PBC ASCs contain AMA.

To assess if liver-infiltrating ASCs are capable of producing disease-associated auto-antibodies, day 14 supernatants from cultured PBC LIMCs of AMA-seropositive patients were tested for PDC-E2 reactivities by indirect immunofluorescence (IF). Using neat PBC supernatant ($n = 3$), AMA staining was very weak (data not shown) therefore we concentrated the supernatants 20-fold using high-molecular weight protein filtration columns [18]. Using concentrated PBC supernatants, we detected weak AMA staining by IF in 1 PBC supernatant sample (PBC 1) and

strong AMA reactivity in 2 samples (PBC 2 and PBC 3, Figure 5A). AMA to PDC-E2 in concentrated PBC supernatants was quantified by ELISA (Table 2) and correlated with IF staining intensities as low levels of AMA to PDC-E2 was measured in PBC 1 (0.6 relative units [RU] /ml), intermediate levels in PBC 2 (34.21 RU/ml) and high levels in PBC 3 (256.25 RU/ml). Concentrated PBC supernatants (3 / 3) were AMA-positive by immunoblotting (IB) whereas ANA reactivities to gp120 and sp100 were absent in 3 / 3 samples (Figure 5B) which was expected as these samples were derived from patients who were ANA-seronegative at diagnosis.

3.6. Liver-infiltrating PSC and PBC ASCs produce auto-antibodies with unique reactivities.

Having established that PSC liver explants contain functional ASCs and liver-infiltrating ASCs in PBC produce disease-specific AMA, we investigated the antibody profile of cultured PSC LIMCs as a means of identifying possible antigenic triggers in PSC. Day 14 supernatants from cultured PSC LIMCs (n = 9) were screened using human full-length protein arrays covering ~74% of the human proteome [2,23]. Using PDC-E2 reactivities in PBC supernatants as a methodological control, we defined positive reactivities ("hits") as having a Z-score $\geq$ 1.5, an Interaction Score (IS) $\geq$ 0.3, a signal-to-noise ratio (S/N) > 2.5 and a standard deviation (SD) between duplicates < 0.25 (Supplementary Figure 2). At these cutoffs, reactivities to PDC-E2 and the putative PBC antigen HK1 [1,2] were detected in 3 / 3 PBC samples cultured from AMA-seropositive explants (Figure 6A) and a total of 218 hits ranging between 3 to 191 per sample were reported (Figure 6B and Supplementary Table 1). PDC-E2 and HK1 were the only antibody targets shared among every PBC sample (3 / 3) and neither reactivity was detected in PSC supernatants (0 / 9). Antibody profiling of PSC samples revealed 98 total hits ranging from 1 to 43 per sample. Eleven of these PSC reactivities were shared among at least 2 samples with auto-antibodies to nucleolar protein 3 (NOL3) detected in 5 / 9, hematopoietic cell-specific Lyn

substrate 1 (HCLS1) in 3 / 9, and adhesion G protein-coupled receptor A3 (ADGRA3), ATPase type 13A5 (ATP13A5), integrin beta-like 1 (ITGBL1), potassium channel tetramerization domain containing 13 (KCTD13), keratin associated protein 5-4 (KRTAP5-4), PRAME family member 12 (PRAMEF12), proline-rich coiled-coil 2B (PRRC2B), serine/arginine-rich splicing factor 1 (SFRS1) and TEA domain family member 3 (TEAD3) in 2 / 9 samples, respectively. None of the reactivities shared among PSC samples were reported in PBC supernatants.

To determine if the auto-antibody reactivities in PSC were biological significant, we assessed if NOL3 auto-antibodies correlated with NOL3 protein expression in matched liver samples. In livers with NOL3 reactivities (PSC 4, 6 – 9), positive NOL3 expression in lymphocytes was detected in 3 / 5 samples and occasional staining in 2 / 5 (Supplementary Figure 1 and Supplementary Table 2). Patchy lymphocyte expression of NOL3 protein was also observed in 3 / 4 PSC livers (PSC 1 – 3) lacking NOL3 antibodies and negative in PSC 5. Lymphocyte expression of NOL3 was occasionally detected in 2 / 3 PBC livers (PBC 2 and PBC 3) and negative in PBC 1. Hepatocytes and the inflammatory interfaces of PSC and PBC livers irrespective of NOL3 reactivities was weak to moderate. NOL3 expression in cholangiocytes was strongest and mainly restricted to the cytoplasm, though some nuclear staining was noted.

4. Discussion

For a majority of autoimmune diseases, auto-antibodies serve as markers of disease activity and may aid in disease diagnosis, as is the case in PBC and CD. In patients with PSC, a large number of auto-antibodies have been reported to date [3,8] however none of these are PSC-specific and epitope mapped. In an effort to better understand PSC, with the goal of improving diagnostics and therapeutics, we hypothesized that liver-infiltrating ASCs in PSC are disease-relevant and capable of producing auto-antibodies that could point to potential triggering antigens and mechanisms of disease.

By combining enzymatic digestion and mechanical disruption of fresh end-stage explants, we found that PSC livers contain substantially fewer plasma cells compared to PBC but total plasmablast numbers were similar. Liver-infiltrating ASCs from PSC and PBC explants were functional and produced similar concentrations of antibodies *in vitro* suggesting that plasmablasts may be the primary source of auto-antibody production in the liver. As plasmablasts are indicative of recent naïve or memory B cell activation [24], these findings also imply that cognate antigen could be constitutively expressed and stimulating continuous plasmablast differentiation in end-stage disease. Similar observations have been reported in PBC where the majority of circulating B cells recognizing PDC-E2 exhibit a plasmablast phenotype ($CD19^{+}CD20^{-}CD27^{+}CD38^{hi}$) [25] but further work using additional ASC markers, such as BLIMP1 [26-28], as well as survival and proliferation studies [24] are necessary as plasma cells may also account for significant auto-antibody production given that plasma cell frequencies in PSC LIMC cultures increased after 2 weeks (Supplementary Figure 8).

In contrast to PBC, PSC is characteristically associated with inflammatory bowel disease (IBD) [4] and pro-inflammatory immune cells are recognized to traffic to the liver from inflamed gut [29]. Moreover it is clear that complex interactions between the intestinal mucosa and associated microbiota includes inflammatory responses to microbial molecules and penetration by intestinal microbes, both of which may be particularly relevant to disease pathogenesis in PSC-IBD [30,31]. Elevated IgA production in IBD has been reported in PSC [32-34] and we detected a higher proportion of IgA-positive plasmablasts in PSC liver and slightly higher IgA concentrations from PSC LIMC cultures compared to PBC. It should be noted that total numbers of IgA-positive ASCs in PSC samples were relatively low compared to the number of IgG-positive and IgM-positive ASCs. This indicates that IgA responses may originate in the gut or appear more strongly at earlier stages of liver inflammation. Based on these results and observations that T cell receptor clonality is shared between gut and liver T cells [35], we propose that disease-relevant ASCs in PSC likely reside in both gut and liver, and may preferentially secrete IgA-positive auto-antibodies.

In addition to immunophenotyping of ASCs, we confirmed that liver-infiltrating ASCs are a source of disease-specific auto-antibodies by demonstrating that culture supernatants from PBC LIMCs show reactivity to PDC-E2. AMA in PBC supernatants were low as IF staining increased substantially using concentrated samples. In 1 / 3 PBC supernatants, AMA to PDC-E2 remained low in concentrated supernatant as measured by IB and ELISA. As this patient was AMA-seropositive, we suspect that disease-specific ASCs may be rare or possibly anergic in some end-stage explants and could require additional activation by cognate antigen or cytokine cocktails to boost antibody production. These results support the study of end-stage explants for disease-

specific antibodies in immune-mediated liver disorders such as PSC. We believe this approach is rational given that the liver is the primary site of active inflammation in PSC, and as several previous studies have assessed PSC serum for disease-specific antibodies [8], the use of end-stage explants represents a novel strategy for the discovery of relevant reactivities.

PSC lacks validated disease-specific antibodies [8] therefore we used recombinant human protein arrays to screen the antibody repertoire of liver-infiltrating ASCs in PSC, applying PDC-E2 reactivity in PBC as a positive control. We detected 11 auto-antibody targets shared among PSC samples, including NOL3 (5 / 9), HCLS1 (3 / 9) and ADGRA3, ATP13A5, ITGBL1, KCTD13, KRTAP5-4, PRAMEF12, PRRC2B, SFRS1 and TEAD3 in 2 / 9 samples. Moderate to high levels of NOL3, ADGRA3, ATP13A5, KCTD13, PRAMEF12, PRRC2B and SFRS1 RNA and protein expression are found in liver [36,37] suggesting these proteins and associated pathways may have links to PSC. The correlation between NOL3 auto-antibodies and protein expression in cholangiocytes from the same liver is provocative given that NOL3 is an anti-apoptotic protein with elevated expression in various cancers [38] and PSC is associated with a significant risk of cholangiocarcinoma [4]. Our findings require robust validation in much large cohorts as the majority of the reactivities detected in PSC and PBC are of unknown disease relevance. These auto-antibodies are most likely to be false positives but may also reflect cross-reactivities to exogenous antigens originating from infectious pathogens or environmental exposures.

Studies such as ours will inevitably be limited by the availability of human diseased liver samples and future work will require that the power and breadth of our investigations are

extended, both within PBC and PSC, and non-biliary related inflammatory disease, such as autoimmune hepatitis. Furthermore, when interpreting array data based on high density platforms quantifying thousands of variables, statistical validation externally is ultimately needed, alongside validation using single cell analyses and blood ASCs. Nevertheless, our study is unique and formative for future work in this field as we have identified liver-infiltrating ASCs as a source disease-specific auto-antibodies which could help define the molecular triggers of PSC and serve as early or prognostic markers of disease.

5. Conclusion

In conclusion, using liver tissue obtained at the time of transplantation from patients with PSC and PBC, we have explored the hypothesis that PSC has a distinct repertoire of liver-infiltrating ASCs and associated auto-antibodies. In so doing, we demonstrate a difference in plasma cell frequency between PSC and PBC, and by identifying AMA to the PBC-specific antigen PDC-E2, confirm the feasibility and specificity of studying liver-infiltrating ASCs as a source of disease-relevant antibodies in PSC.

Acknowledgements

B.K.C is supported by the European Union Seventh Framework Programme (FP7-PEOPLE-2013-COFUND) under grant agreement #609020 (Scientia Fellows). D.G.U would like to thank the Helse Sør-Øst (Project #2015024) for financial support. B.K.C, Z.S, G.M.H and E.L have received support from the NIHR Liver Biomedical Research Unit. We thank Matthew Taylor, Abid Karim and Tim Plant of the Clinical Immunology Service at the University of Birmingham for measuring AMA reactivity and Niamh Quann from the University of Hospitals Birmingham NHS Foundation Trust for clinical data.

This paper presents independent research supported by the NIHR Birmingham Liver Biomedical Research Unit based at the University Hospitals Birmingham NHS Foundation Trust and the University of Birmingham. The views expressed in this publication are those of the authors and not necessarily those of the NHS, the NIHR or the Department of Health.

References

[1] G.L. Norman, C.-Y. Yang, H.P. Ostendorff, Z. Shums, M.J. Lim, J. Wang, et al., Anti-kelch-like 12 and anti-hexokinase 1: novel autoantibodies in primary biliary cirrhosis, Liver International. 35 (2014) 642–651. doi:10.1111/liv.12690.

[2] C.J. Hu, G. Song, W. Huang, G.Z. Liu, C.W. Deng, H.P. Zeng, et al., Identification of New Autoantigens for Primary Biliary Cirrhosis Using Human Proteome Microarrays, Mol. Cell Proteomics. 11 (2012) 669–680. doi:10.1074/mcp.M111.015529.

[3] T.H. Karlsen, B.K. Chung, Genetic Risk and the Development of Autoimmune Liver Disease, Dig Dis. 33 Suppl 2 (2015) 13–24. doi:10.1159/000440706.

[4] G.M. Hirschfield, T.H. Karlsen, K.D. Lindor, D.H. Adams, Primary sclerosing cholangitis, Lancet. 382 (2013) 1587–1599. doi:10.1016/S0140-6736(13)60096-3.

[5] G.M. Hirschfield, M.E. Gershwin, The Immunobiology and Pathophysiology of Primary Biliary Cirrhosis, Annu. Rev. Pathol. Mech. Dis. 8 (2013) 303–330. doi:10.1146/annurev-pathol-020712-164014.

[6] G.M. Hirschfield, X. Liu, Y. Han, I.P. Gorlov, Y. Lu, C. Xu, et al., Variants at IRF5-TNPO3, 17q12-21 and MMEL1 are associated with primary biliary cirrhosis, Nature Publishing Group. 42 (2010) 655–657. doi:10.1038/ng.631.

[7] Y. Okada, K. Kim, B. Han, N.E. Pillai, R.T.-H. Ong, W.-Y. Saw, et al., Risk for ACPA-positive rheumatoid arthritis is driven by shared HLA amino acid polymorphisms in Asian and European populations, Hum. Mol. Genet. 23 (2014) 6916–6926. doi:10.1093/hmg/ddu387.

[8] J.R. Hov, K.M. Boberg, T.H. Karlsen, Autoantibodies in primary sclerosing cholangitis, World J. Gastroenterol. 14 (2008) 3781–3791.

[9] E. Melum, A. Franke, C. Schramm, T.J. Weismüller, D.N. Gotthardt, F.A. Offner, et al., Genome-wide association analysis in primary sclerosing cholangitis identifies two non-HLA susceptibility loci, Nature Publishing Group. 43 (2011) 17–19. doi:10.1038/ng.728.

[10] J.Z. Liu, J.R. Hov, T. Folseraas, E. Ellinghaus, S.M. Rushbrook, N.T. Doncheva, et al., Dense genotyping of immune-related disease regions identifies nine new risk loci for primary sclerosing cholangitis, Nature Publishing Group. 45 (2013) 670–675. doi:10.1038/ng.2616.

[11] T.H. Karlsen, A. Franke, E. Melum, A. Kaser, J.R. Hov, T. Balschun, et al., Genome-wide association analysis in primary sclerosing cholangitis, Gastroenterology. 138 (2010) 1102–1111. doi:10.1053/j.gastro.2009.11.046.

[12] D. Cabibi, G. Tarantino, F. Barbaria, M. Campione, A. Craxì, V. Di Marco, Intrahepatic IgG/IgM plasma cells ratio helps in classifying autoimmune liver diseases, Dig Liver Dis. 42 (2010) 585–592. doi:10.1016/j.dld.2009.12.006.

[13] R.K. Moreira, F. Revetta, E. Koehler, M.K. Washington, Diagnostic utility of IgG and IgM immunohistochemistry in autoimmune liver disease, World J. Gastroenterol. 16 (2010) 453–457.

[14] R.P. Myers, M.G. Swain, S.S. Lee, A.A.M. Shaheen, K.W. Burak, B-Cell Depletion With Rituximab in Patients With Primary Biliary Cirrhosis Refractory to Ursodeoxycholic Acid, Am. J. Gastroenterol. 108 (2013) 933–941. doi:10.1038/ajg.2013.51.

[15] P. Suwannalai, H.U. Scherer, D. van der Woude, A. Ioan-Facsinay, C.M. Jol-van der Zijde, M.J.D. van Tol, et al., Anti-citrullinated protein antibodies have a low avidity compared with antibodies against recall antigens, Ann. Rheum. Dis. 70 (2011) 373–379.

doi:10.1136/ard.2010.135509.

[16] H. Huang, C. Benoist, D. Mathis, Rituximab specifically depletes short-lived autoreactive plasma cells in a mouse model of inflammatory arthritis, Proceedings of the National Academy of Sciences. 107 (2010) 4658–4663. doi:10.1073/pnas.1001074107.

[17] G.M. Reynolds, L.J. Billingham, L.J. Gray, J.R. Flavell, S. Najafipour, J. Crocker, et al., Interleukin 6 expression by Hodgkin/Reed-Sternberg cells is associated with the presence of 'B' symptoms and failure to achieve complete remission in patients with advanced Hodgkin's disease, British Journal of Haematology. 118 (2002) 195–201.

[18] K. Saha, R. Case, P.K. Wong, A simple method of concentrating monoclonal antibodies from culture supernatant by ultrafiltration, J. Immunol. Methods. 151 (1992) 307–308.

[19] P. Farci, G. Diaz, Z. Chen, S. Govindarajan, A. Tice, L. Agulto, et al., B cell gene signature with massive intrahepatic production of antibodies to hepatitis B core antigen in hepatitis B virus-associated acute liver failure, Proceedings of the National Academy of Sciences. 107 (2010) 8766–8771. doi:10.1073/pnas.1003854107.

[20] L. Mesin, R. Di Niro, K.M. Thompson, K.E.A. Lundin, L.M. Sollid, Long-Lived Plasma Cells from Human Small Intestine Biopsies Secrete Immunoglobulins for Many Weeks In Vitro, The Journal of Immunology. 187 (2011) 2867–2874. doi:10.4049/jimmunol.1003181.

[21] D.A. Kaminski, C. Wei, Y. Qian, A.F. Rosenberg, I. Sanz, Advances in human B cell phenotypic profiling, Front Immunol. 3 (2012) 302. doi:10.3389/fimmu.2012.00302.

[22] M. Cocco, S. Stephenson, M.A. Care, D. Newton, N.A. Barnes, A. Davison, et al., In vitro generation of long-lived human plasma cells, The Journal of Immunology. 189 (2012) 5773–5785. doi:10.4049/jimmunol.1103720.

[23] J.S. Jeong, L. Jiang, E. Albino, J. Marrero, H.S. Rho, J. Hu, et al., Rapid identification of

monospecific monoclonal antibodies using a human proteome microarray, Mol. Cell Proteomics. 11 (2012) O111.016253. doi:10.1074/mcp.O111.016253.

[24] S.L. Nutt, P.D. Hodgkin, D.M. Tarlinton, L.M. Corcoran, The generation of antibody-secreting plasma cells, Nat. Rev. Immunol. 15 (2015) 160–171. doi:10.1038/nri3795.

[25] J. Zhang, W. Zhang, P.S.C. Leung, C.L. Bowlus, S. Dhaliwal, R.L. Coppel, et al., Ongoing activation of autoantigen-specific B cells in primary biliary cirrhosis, Hepatology. 60 (2014) 1708–1716. doi:10.1002/hep.27313.

[26] P.G. Soro, P. Morales-A, J.A. Martínez-M, S. Morales-A, S.G. Copín, M.A. Marcos, et al., Differential involvement of the transcription factor Blimp-1 in T cell-independent and -dependent B cell differentiation to plasma cells, J. Immunol. 163 (1999) 611–617.

[27] C. Angelin-Duclos, G. Cattoretti, K.I. Lin, K. Calame, Commitment of B lymphocytes to a plasma cell fate is associated with Blimp-1 expression in vivo, J. Immunol. 165 (2000) 5462–5471.

[28] A. Kallies, J. Hasbold, D.M. Tarlinton, W. Dietrich, L.M. Corcoran, P.D. Hodgkin, et al., Plasma cell ontogeny defined by quantitative changes in blimp-1 expression, J. Exp. Med. 200 (2004) 967–977. doi:10.1084/jem.20040973.

[29] B. Eksteen, The Gut-Liver Axis in Primary Sclerosing Cholangitis, Clinics in Liver Disease. 20 (2016) 1–14. doi:10.1016/j.cld.2015.08.012.

[30] M. Kummen, K. Holm, J.A. Anmarkrud, S. Nygård, M. Vesterhus, M.L. Høivik, et al., The gut microbial profile in patients with primary sclerosing cholangitis is distinct from patients with ulcerative colitis without biliary disease and healthy controls, Gut. (2016). doi:10.1136/gutjnl-2015-310500.

[31] M.N. Quraishi, M. Sergeant, G. Kay, T. Iqbal, J. Chan, C. Constantinidou, et al., The gut-adherent microbiota of PSC–IBD is distinct to that of IBD, Gut. (2016) gutjnl–2016–

311915. doi:10.1136/gutjnl-2016-311915.

[32] M. Heydtmann, P.F. Lalor, J.A. Eksteen, S.G. Hübscher, M. Briskin, D.H. Adams, CXC chemokine ligand 16 promotes integrin-mediated adhesion of liver-infiltrating lymphocytes to cholangiocytes and hepatocytes within the inflamed human liver, J. Immunol. 174 (2005) 1055–1062.

[33] Y.H. Oo, V. Banz, D. Kavanagh, E. Liaskou, D.R. Withers, E. Humphreys, et al., CXCR3-dependent recruitment and CCR6-mediated positioning of Th-17 cells in the inflamed liver, J. Hepatol. 57 (2012) 1044–1051. doi:10.1016/j.jhep.2012.07.008.

[34] L. Berglin, N.K. Björkström, A. Bergquist, Primary sclerosing cholangitis is associated with autoreactive IgA antibodies against biliary epithelial cells, Scand. J. Gastroenterol. 48 (2015) 719–728. doi:10.3109/00365521.2013.786131.

[35] E. Liaskou, E.K.K. Henriksen, K. Holm, F. Kaveh, D. Hamm, J. Fear, et al., High-throughput T-cell receptor sequencing across chronic liver diseases reveals distinct disease-associated repertoires, Hepatology. (2015). doi:10.1002/hep.28116.

[36] M. Uhlén, P. Oksvold, L. Fagerberg, E. Lundberg, K. Jonasson, M. Forsberg, et al., Towards a knowledge-based Human Protein Atlas, Nat. Biotechnol. 28 (2010) 1248–1250. doi:10.1038/nbt1210-1248.

[37] M. Uhlén, L. Fagerberg, B.M. Hallström, C. Lindskog, P. Oksvold, A. Mardinoglu, et al., Proteomics. Tissue-based map of the human proteome, Science. 347 (2015) 1260419. doi:10.1126/science.1260419.

[38] M. Wang, S. Qanungo, M.T. Crow, M. Watanabe, A.-L. Nieminen, Apoptosis repressor with caspase recruitment domain (ARC) is expressed in cancer cells and localizes to nuclei, FEBS Lett. 579 (2005) 2411–2415. doi:10.1016/j.febslet.2005.03.040.

TABLES

Table 1. Clinical characteristics of the study cohort

Clinical Characteristic	PSC (n = 25)	PBC (n = 13)
Median age (years)	51	53
Range	(17-72)	(32-72)
Sex Distribution (M:F)		
Male	14	1
Female	11	10
Serum Auto-antibodies		
AMA-positive	0 / 24	8 / 10
ANA-positive	12 / 24	2 / 11
ANCA-positive	10 / 20	2 / 9
Serum Immunoglobulin (median g / L)		
IgA	3.9 ± 0.6	3.4 ± 0.8
IgG	16.4 ± 1.6	16.6 ± 2.2
IgM	1.9 ± 0.2	3.2 ± 1.0

Table 2. Concentration of AMA to PDC-E2 in day 14 supernatant from cultured PBC LIMCs.

	AMA to PDC-E2		
Sample	**Immunofluorescence**	**Immunoblot**	**ELISA** (relative units/ml)
PBC 1	+	+	0.6
PBC 2	+ + / + + +	+ + +	34.21
PBC 3	+ + +	+ + +	256.26

Figure 1.

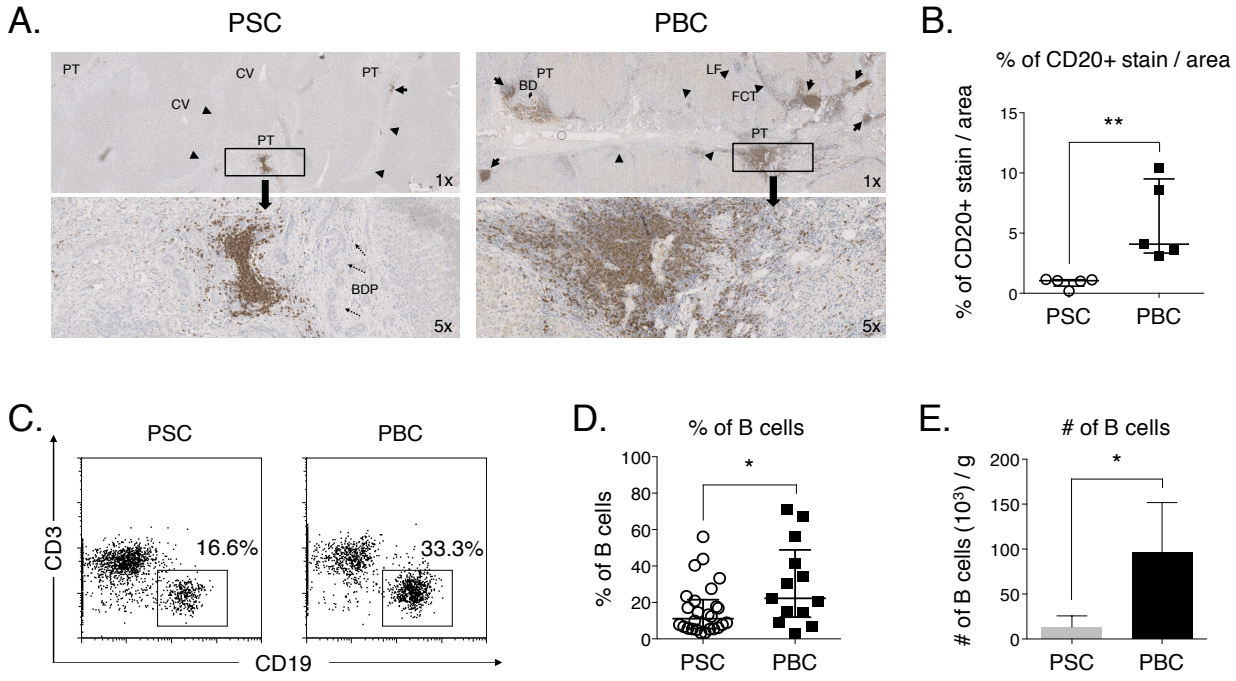
A.
PSC
PBC
PT
CV
PT
CV
PT
1x
BDP
5x
PT
BD
LF
FCT
PT
1x
5x
B.
% of CD20+ stain / area
% of CD20+ stain / area
15
10
5
0
**
PSC
PBC
C.
PSC
PBC
CD3
16.6%
33.3%
CD19
D.
% of B cells
% of B cells
100
80
60
40
20
0
*
PSC
PBC
E.
# of B cells
# of B cells (10³) / g
200
150
100
50
0
*
PSC
PBC

Figure 2.

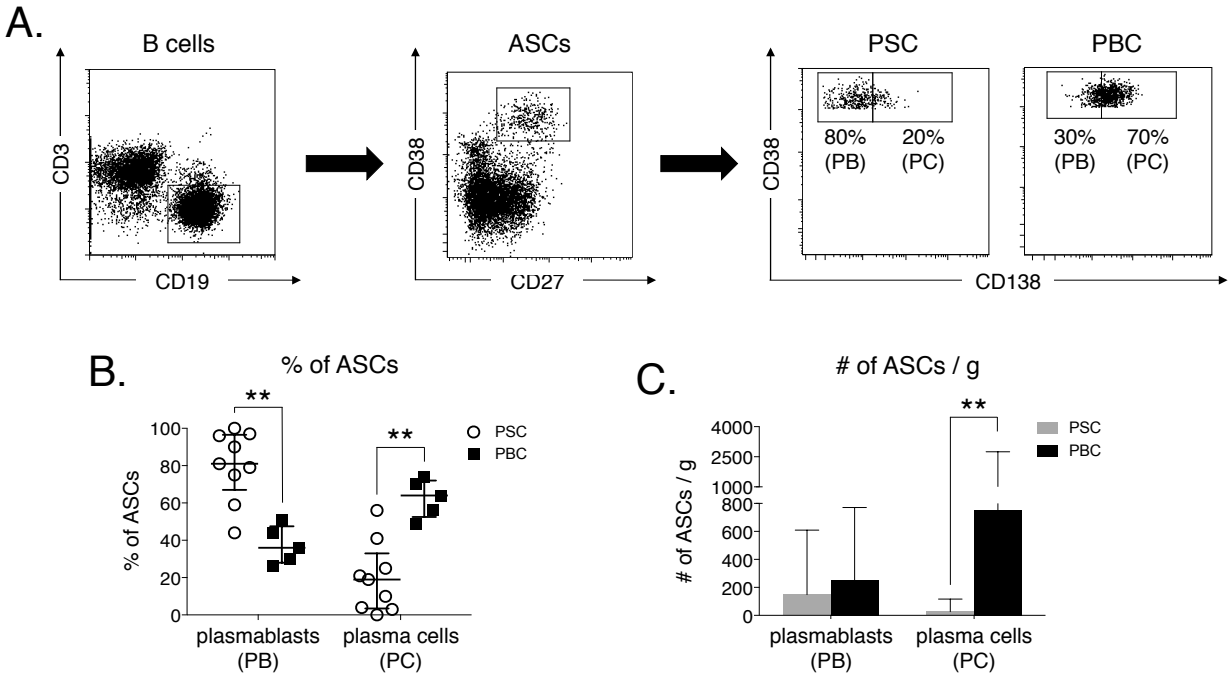
A.
B cells
CD3
CD19
ASCs
CD38
CD27
PSC
PBC
80%
(PB)
20%
(PC)
30%
(PB)
70%
(PC)
CD38
CD138
B.
% of ASCs
**
**
PSC
PBC
% of ASCs
100
80
60
40
20
0
plasmablasts
(PB)
plasma cells
(PC)
C.
# of ASCs / g
**
PSC
PBC
# of ASCs / g
4000
2500
1000
800
600
400
200
0
plasmablasts
(PB)
plasma cells
(PC)

Figure 3.

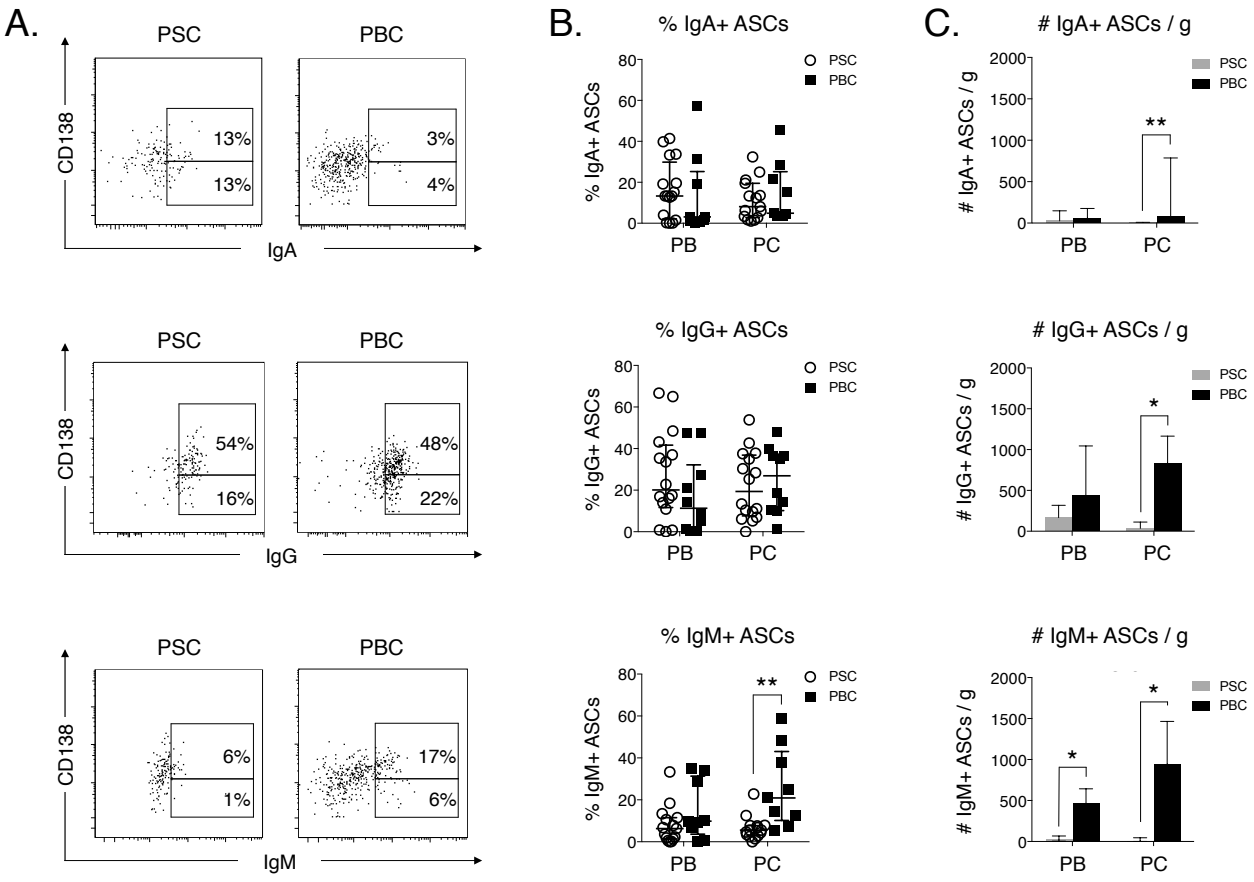
A.
PSC
PBC
CD138
IgA
13%
13%
3%
4%
IgG
54%
16%
48%
22%
IgM
6%
1%
17%
6%
B.
% IgA+ ASCs
% IgG+ ASCs
% IgM+ ASCs
PSC
PBC
PB
PC
C.
IgA+ ASCs / g
IgG+ ASCs / g
IgM+ ASCs / g

Figure 4.

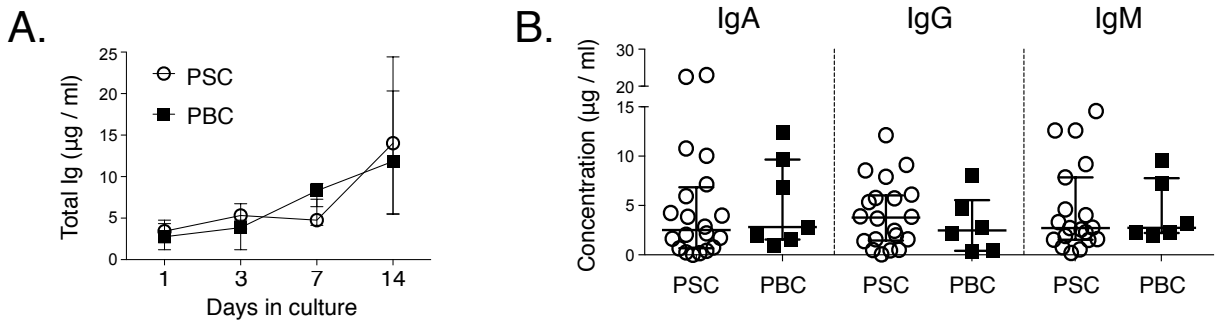
A.
Total Ig (µg / ml)
PSC
PBC
Days in culture
B.
IgA
IgG
IgM
Concentration (µg / ml)
PSC
PBC

Figure 5.

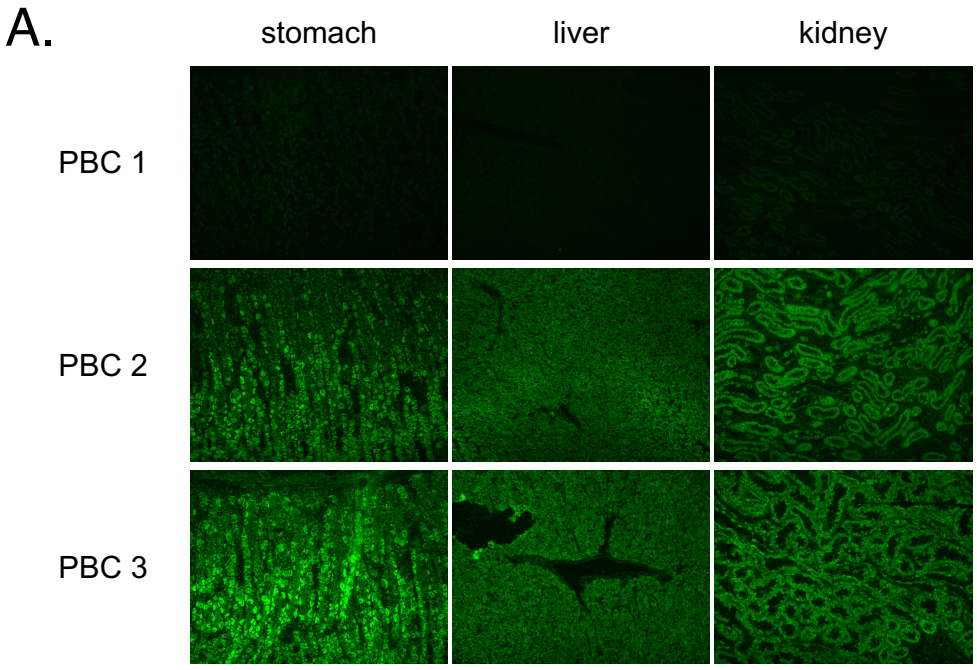
A.
stomach
liver
kidney
PBC 1
PBC 2
PBC 3

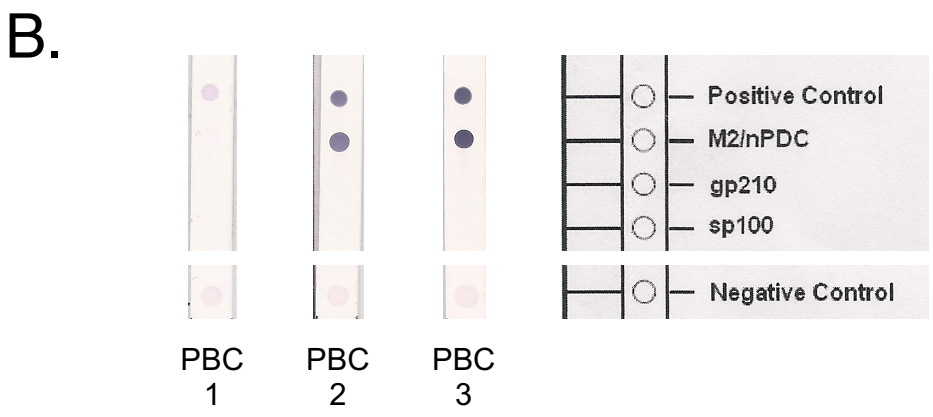
B.
Positive Control
M2/nPDC
gp210
sp100
Negative Control
PBC 1
PBC 2
PBC 3

Figure 6.

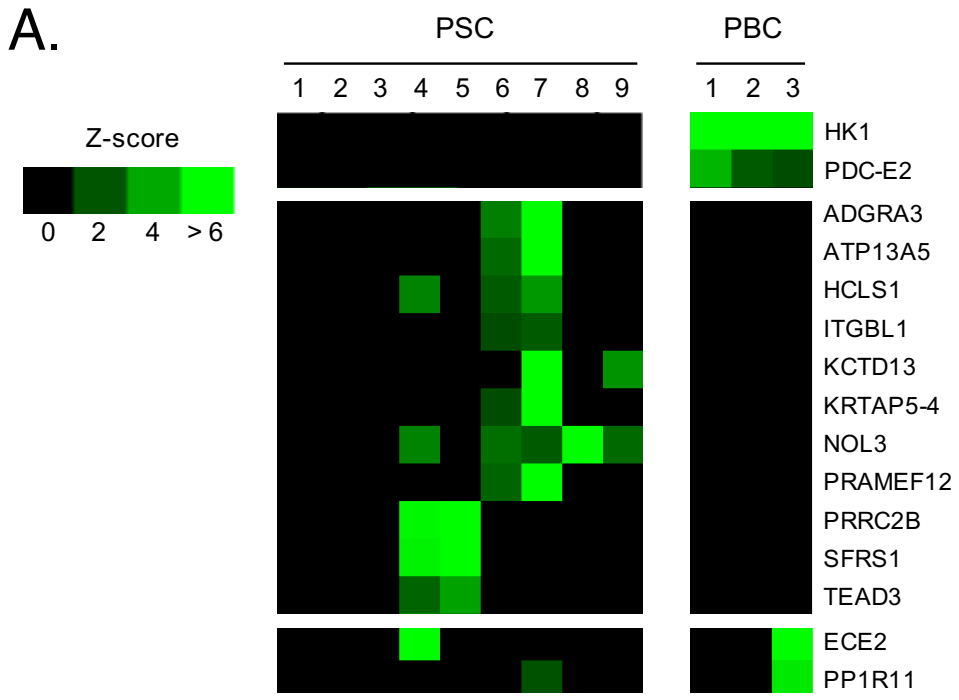
A.
PSC
PBC
1 2 3 4 5 6 7 8 9
1 2 3
Z-score
0 2 4 > 6
HK1
PDC-E2
ADGRA3
ATP13A5
HCLS1
ITGBL1
KCTD13
KRTAP5-4
NOL3
PRAMEF12
PRRC2B
SFRS1
TEAD3
ECE2
PP1R11

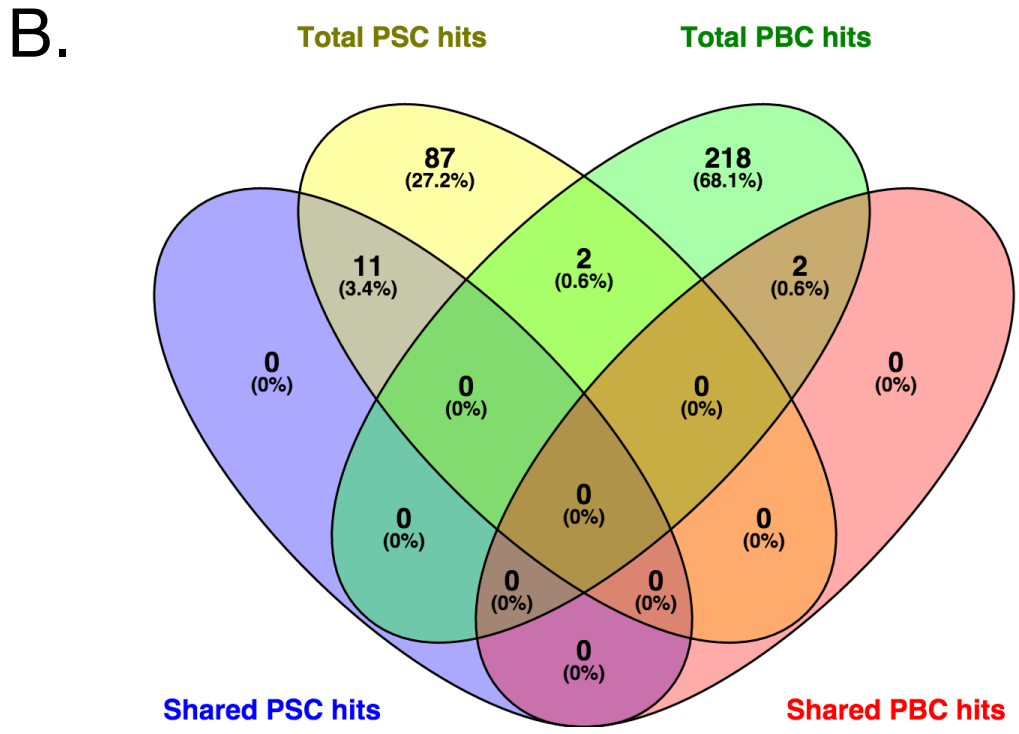
B.
Total PSC hits
Total PBC hits
87 (27.2%)
218 (68.1%)
11 (3.4%)
2 (0.6%)
2 (0.6%)
0 (0%)
0 (0%)
0 (0%)
0 (0%)
0 (0%)
0 (0%)
0 (0%)
0 (0%)
0 (0%)
0 (0%)
Shared PSC hits
Shared PBC hits

SUPPLEMENTARY MATERIAL FOR REVIEW

SUPPLEMENTARY TABLE LEGEND

Supplementary Table 1. Auto-antibody targets detected in culture supernatant (day 14) of LIMCs enriched from PSC (n = 9) and PBC (n = 3) explants. The Z-score and Interaction Score (IS) is given for each antibody target with a Z-score ≥ 1.5, IS ≥ 0.3 and standard deviation (SD) between duplicates < 0.25.

Supplementary Table 2. Immunostaining for nucleolar protein 3 (NOL3) expression in PSC (n = 9) and PBC (n = 3) liver explants. Cultured LIMC supernatants (day 14) from each explant (PSC 1 – 9 and PBC 1 – 3) were tested for NOL3 antibodies by protein array analysis (+ ; positive, – ; negative). NOL3 expression in lymphocytes was graded as negative, occasional or positive. Cholangiocyte and hepatocyte NOL3 expression was graded as weak (+), moderate (++) or strong (+++) based on IgG negative control and positive control staining of muscle present in the liver vasculature (Supplementary Figure 1).

SUPPLEMENTARY FIGURE LEGENDS

Supplementary Figure 1. NOL3 protein expression is observed in end-stage PSC and PBC liver explants by immunostaining.

PSC and PBC liver tissues were immunostained for NOL3 and counterstained with haematoxylin. (**A**) Representative NOL3 staining indicates heterogeneous cytoplasmic NOL3 expression in hepatocytes [H] ranging from negative [A] to weak (+) intensity [B], and moderate (++) staining [C] at the inflammatory interfaces [II] in some cases. NOL3 expression around bile ducts [BD] and in cholangiocytes [D] was generally uniform and moderate to strong (++ / +++). Muscle surrounding the liver vasculature [V] served as internal positive controls and demonstrated moderate cytoplasmic and strong nuclear staining [E]. (**B**) Representative weak cytoplasmic NOL3 staining of hepatocytes [H] and strong staining of bile ducts [BD]. Positive NOL3 staining of lymphocytes is noticeably present and indicated with arrows. (**C**) Representative moderate to strong NOL3 staining of larger bile ducts [BD] and negative NOL3 staining of hepatocytes [H]. (**D**) NOL3 staining of pre-cirrhotic regions typically showed weak cytoplasmic staining of hepatocytes [H] and moderate staining of bile ducts [BD] and cholangiocytes.

Supplementary Figure 2. Workflow of protein array analysis.

LIMCs enriched from PSC (n = 9) and PBC (n = 9) explants were cultured for 14 days and supernatants were assessed for auto-antibodies using the indicated workflow. $F_{protein}$ = sample fluorescence of specific protein, $F_{average}$ = mean fluorescence of total protein array excluding

control spots, SD = standard deviation, $F_{GST\text{-}protein}$ = fluorescence intensity of specific protein using anti-GST antibody.

Supplementary Figure 3. Total numbers of LIMCs are reduced in PSC explants compared to PBC.

LIMCs isolated using a combination of enzymatic and mechanical digestion from fresh PSC (n = 11) and PBC explants (n = 6) were counted manually using a hemocytometer. Median number (#) of LIMCs per gram (g) of explanted tissue is shown and error bars represent interquartile range, p = 0.52.

Supplementary Figure 4. PSC and PBC explants contain similar proportions of antibody-secreting B cells (ASCs).

LIMCs from PSC and PBC explants were stained with viability dye and anti-human CD3, CD19, CD27 and CD38 antibodies (or isotype controls) and analyzed by flow cytometry. (**A**) Representative flow cytometry plots indicate the proportion (%) of ASCs ($CD27+CD38^{hi}$ B cells) within the viable B cell subset of PSC and PBC explants. (**B**) Cumulative proportion (%) of ASCs within the viable B cell subset of PSC (n = 28) and PBC (n = 12) samples.

Supplementary Figure 5. Similar proportions of IgA+, IgG+ and IgM+ B cells are detected by surface and intracellular staining.

LIMCs from PSC and PBC explants were stained with viability dye and anti-human CD3, CD19, CD138, IgA, IgG and IgM. Representative flow cytometry plots indicate the frequency (%) of viable IgA+, IgG+ and IgM+ CD138+ and CD138– B cells from a PSC (**A**) and PBC (**B**) explant with surface Ig staining or combined surface and intracellular (intra) Ig staining.

Supplementary Figure 6. Cultured ASCs from a subset of PSC explants produce high concentrations of IgA.

LIMCs containing ASCs were enriched from PSC explants (n = 21) were cultured for 14 days and concentrations of supernatant IgG were measured by ELISA performed in triplicate, $^{**}p < 0.01$.

Supplementary Figure 7. Antibody production by cultured LIMCs does not correlate with serum antibody concentrations.

LIMCs containing ASCs were enriched from PSC (n = 15) and PBC (n = 6) explants and cultured for 14 days. Concentrations of IgA, IgG and IgM in the supernatant of cultured PSC (**A**) and PBC (**B**) LIMCs were measured by ELISA performed in triplicate and matched to serum IgA, IgG and IgM concentrations from the same patient assessed prior to liver transplantation.

Supplementary Figure 8. Plasma cell frequencies increase in cultured PSC and PBC LIMCs.

LIMCs enriched from PSC and PBC explants were cultured for 14 days and stained with anti-human CD3, CD19, CD27, CD38 and CD138. (**A**) Representative flow cytometry plots indicate the frequency (%) of viable plasmablasts (PB; CD19+CD27+CD38^{hi}CD138–) and plasma cells (PC; CD19+CD27+CD38^{hi}CD138+) within the total ASC population (CD19+CD27+CD38^{hi}). Positive CD138 staining was determined using a matched isotype control (not shown). (**B**) Dot plots indicate the frequency (%) of viable plasmablasts (PB) and plasma cells (PC) after 14 days of culture. The median frequency of the plasmablast and plasma cell subsets from PSC (n = 6 - 10) and PBC samples (n = 3 - 4) is shown. Error bars represent interquartile range among samples, *p = 0.05.

SUPPLEMENTARY MATERIAL – TABLE 1

Sample	Target	Gene name	Z-score	IS
PSC 001	GORASP1	golgi reassembly stacking protein 1	9.6	1.7
PSC 001	BEAN1	brain expressed associated with NEDD4, 1	2.6	0.5

Sample	Target	Gene name	Z-score	IS
PSC 002	ANKRD28	ankyrin repeat domain 28	15.1	2.7
PSC 002	CHAC2	ChaC, cation transport regulator homolog 2 (E. coli)	6.6	1.2
PSC 002	GAB1	GRB2 associated binding protein 1	1.7	0.3

Sample	Target	Gene name	Z-score	IS
PSC 003	SULT2B1	sulfotransferase family, cytosolic, 2B, member 1	3.2	0.5

Sample	Target	Gene name	Z-score	IS
PSC 004	LCMT1	leucine carboxyl methyltransferase 1	34.8	132.2
PSC 004	ALG12	ALG12, alpha-1,6-mannosyltransferase	18.0	24.7
PSC 004	RNF216P1	ring finger protein 216 pseudogene 1	17.5	93.8
PSC 004	ZNF385B	zinc finger protein 385B	12.9	58.0
PSC 004	SDCBP	syndecan binding protein (syntenin)	12.0	50.8
PSC 004	ITGB1BP2	integrin beta 1 binding protein (melusin) 2	11.5	2.3
PSC 004	ZNF385A	zinc finger protein 385A	9.9	72.3
PSC 004	SF3B4	splicing factor 3b, subunit 4, 49kDa	8.3	1.9
PSC 004	TPM3	tropomyosin 3	7.5	2.1
PSC 004	PDK2	pyruvate dehydrogenase kinase 2	6.9	9.8
PSC 004	SNRK	SNF related kinase	6.6	3.2
PSC 004	TTN	titin	6.4	1.7

PSC 004	RBM12	RNA binding motif protein 12	6.3	1.3
PSC 004	ECE2	endothelin converting enzyme 2	5.8	1.7
PSC 004	TSR3	TSR3, 20S rRNA accumulation, homolog	5.4	4.4
PSC 004	IFI6	interferon, alpha-inducible protein 6	5.2	80.2
PSC 004	PRRC2B	proline-rich coiled-coil 2B	4.9	1.0
PSC 004	FAM84A	family with sequence similarity 84, member A	4.9	1.5
PSC 004	FABP5	fatty acid binding protein 5 (psoriasis-associated)	4.9	1.3
PSC 004	SFRS1	serine/arginine-rich splicing factor 1	4.8	57.0
PSC 004	CSTF2T	cleavage stimulation factor, 3' pre-RNA, subunit 2, tau variant	3.6	0.8
PSC 004	DLG3	discs, large homolog 3 (*Drosophila*)	3.5	1.2
PSC 004	AAMP	angio-associated, migratory cell protein	3.3	2.6
PSC 004	PCBP2	poly(RC) binding protein 2	3.3	0.5
PSC 004	ARHGEF19	Rho guanine nucleotide exchange factor (GEF) 19	3.1	12.2
PSC 004	BAK1	BCL2-antagonist/killer 1	3.1	3.3
PSC 004	SH3GL2	SH3-domain GRB2-like 2	3.0	0.9
PSC 004	OGFOD3	2-oxoglutarate + iron-dependent oxygenase domain 3	2.9	4.6
PSC 004	NOL3	nucleolar protein 3	2.6	1.2
PSC 004	HCLS1	hematopoietic cell-specific Lyn substrate 1	2.6	1.2
PSC 004	SET	SET nuclear proto-oncogene	2.5	1.5
PSC 004	DDX58	DEAD (Asp-Glu-Ala-Asp) box polypeptide 58	2.4	5.0
PSC 004	PAF1	PAF homolog, Paf1/RND polymerase II complex component	2.4	0.7
PSC 004	MGP	matrix Gla protein	2.3	3.8
PSC 004	SPEG	SPEG completx locus	2.1	4.6
PSC 004	PPP5C	protein phosphatase 5 catalytic subunit	2.1	0.7
PSC 004	TEAD3	TEA domain transcription factor 3	2.0	1.2
PSC 004	COPB2	coatomer protein complex subunit beta 2	1.9	2.5
PSC 004	ATP8B5P	ATPase phospholipid transporting 8B5, pseudogene	1.8	1.6
PSC 004	CCDC155	coiled-coil domain containing 155	1.8	1.0
PSC 004	LIMS1	LIM zinc finger domain containing 1	1.7	16.3

PSC 004	GTPBP6	GTP binding protein 6	1.7	11.0
PSC 004	FIZ1	FLT3 interacting zinc finger 1	1.5	106.3

Sample	**Target**	**Gene name**	**Z-score**	**IS**
PSC 005	TAC3	tachykinin 3	42.2	87.8
PSC 005	CLIC4	chloride intracellular channel 4	31.3	13.0
PSC 005	PPP1R3C	protein phosphatase 1, regulatory subunit 3C	28.8	71.5
PSC 005	PRRC2B	proline-rich coiled-coil 2B	12.4	2.3
PSC 005	LSM12	LSM12 homolog	12.1	4.4
PSC 005	TRGV9	T cell receptor gamma variable 9	6.7	15.2
PSC 005	SFRS1	serine/arginine-rich splicing factor 1	6.6	62.4
PSC 005	C1orf94	chromosome 1 open reading frame 94	6.0	2.5
PSC 005	LINC01465	long intergenic non-protein coding RNA 1465	5.4	3.9
PSC 005	LGALS13	lectin, galactoside-binding, soluble, 13	5.1	1.1
PSC 005	BEGAIN	brain enriched guanylate kinase associated	4.7	7.4
PSC 005	PDC	phosducin	4.5	1.0
PSC 005	CEP72	centrosomal protein 72kDa	4.3	8.8
PSC 005	CNN2	calponin 2	4.1	15.7
PSC 005	WARS	tryptophanyl-tRNA synthetase	4.0	1.2
PSC 005	SSBP3	single stranded DNA binding protein 3	3.7	3.3
PSC 005	TXNRD1	thioredoxin reductase 1	3.6	0.9
PSC 005	BRF1	transcription factor TFIIIB subunit BRF1	3.4	91.1
PSC 005	MCM6	minichromosome maintenance complex component 6	3.4	3.4
PSC 005	SSBP2	singel stranded DNA binding protein 2	3.3	4.5
PSC 005	TEAD3	TEA domain transcription factor 3	3.2	1.6
PSC 005	TES	testin LIM domain protein	2.8	0.6
PSC 005	GPR31	G protein-coupled receptor 31	2.8	52.6
PSC 005	HK3	hexokinase 3	2.7	0.8
PSC 005	GLRX3	glutaredoxin 3	2.6	0.7

PSC 005	LIMD1	LIM domains containing 1	2.2	0.5
PSC 005	MBTPS1	membrane bound transcription factor peptidase, site 1	2.0	6.0
PSC 005	MYLK2	myosin light chai kinase 2	1.9	11.6
PSC 005	LTC4S	leukotriene C4 synthase	1.9	3.6
PSC 005	POGZ	pogo transposable element with ZNF domain	1.7	1.0
PSC 005	MC1R	melancortin 1 receptor	1.7	17.9
PSC 005	TAPBP	TAP binding protein	1.5	3.0

Sample	**Target**	**Gene name**	**Z-score**	**IS**
PSC 006	ADGRA3	adhesion G protein-coupled receptor A3	2.5	41.1
PSC 006	NOL3	nucleolar protein 3	2.2	0.4
PSC 006	ATP13A5	ATPase type 13A5	2.1	10.0
PSC 006	PRAMEF12	PRAME family member 12	2.0	2.2
PSC 006	PRKAR1B	protein kinase cAMP-dependent type I regulatory subunit beta	2.0	0.3
PSC 006	XKRY	XK related, Y-linked	1.8	0.4
PSC 006	HCLS1	hematopoietic cell-specific Lyn substrate 1	1.8	0.3
PSC 006	KRTAP5-4	keratin associated protein 5-4	1.5	1.4
PSC 006	ITGBL1	integrin subunit beta like 1	1.5	1.5

Sample	**Target**	**Gene name**	**Z-score**	**IS**
PSC 007	GSN	gelsolin	8.1	1.4
PSC 007	ATP13A5	ATPase type 13A5	8.0	39.4
PSC 007	ADGRA3	adhesion G protein-coupled receptor A3	7.3	119.3
PSC 007	KCTD13	potassium channel tetramerization domain containing 13	7.0	30.6
PSC 007	PRAMEF12	PRAME family member 12	6.3	7.3
PSC 007	TIGD1	tigger transposable element derived 1	5.8	5.7
PSC 007	KRTAP5-4	keratin associated protein 5-4	5.2	3.6
PSC 007	KRTAP5-2	keratin associated protein 5-2	4.0	0.8

PSC 007	KRTAP5-8	keratin associated protein 5-8	3.9	0.8
PSC 007	KRTAP5-1	keratin associated protein 5-1	3.7	1.1
PSC 007	SLC39A7	solute carrier family 39 (zinc transporter), member 7	3.2	8.6
PSC 007	LCN15	lipocalin 15	3.0	1.1
PSC 007	HCLS1	hematopoietic cell-specific Lyn substrate 1	3.0	0.6
PSC 007	SOCS1	suppressor of cytokine signaling 1	2.8	1.1
PSC 007	AKIRIN2	akirin 2	2.8	0.8
PSC 007	FAN1	FANCD2/FANCI-associated nuclease 1	2.7	7.9
PSC 007	KRTAP5-11	keratin associated protein 5-11	2.5	0.4
PSC 007	NOL3	nucleolar protein 3	1.8	0.3
PSC 007	ITGBL1	integrin subunit beta like 1	1.8	2.2
PSC 007	PPP1R11	protein phosphatase 1 regulatory inhibitor subunit 11	1.6	0.3

Sample	**Target**	**Gene name**	**Z-score**	**IS**
PSC 008	SNAP47	synaptosome associated protein 47kDa	81.4	37.1
PSC 008	NOL3	nucleolar protein 3	5.2	0.9

Sample	**Target**	**Gene name**	**Z-score**	**IS**
PSC 009	KCTD13	potassium channel tetramerization domain containing 13	2.9	14.2
PSC 009	ANKHD1	ankyrin repeat and KH domain containing 1	2.8	0.5
PSC 009	NOL3	nucleolar protein 3	2.1	0.3

Sample	**Target**	**Gene name**	**Z-score**	**IS**
PBC 001	HK1	hexokinase 1	7.3	8.5
PBC 001	PDC-E2	dihydrolipoamide S-acetyltransferase	3.6	37.0
PBC 001	CTSB	cathepsin B	1.5	63.6

Sample	Target	Gene name	Z-score	IS
PBC 002	HK1	hexokinase 1	11.7	2.8
PBC 002	STARD4	StAR-related lipid transfer (START) domain containing 4	4.5	0.7
PBC 002	HNRPA0	heterogeneous nuclear ribnucleoprotein A0	2.9	39.5
PBC 002	RABL2B	RAB, member of RAS oncogene family-like 2B	2.7	31.4
PBC 002	IFT22	intraflagellar transport 22	2.6	2.4
PBC 002	KRAS	Kirsten rat sarcoma viral oncogene homolog	2.5	15.5
PBC 002	LAD1	ladinin 1	2.5	1.4
PBC 002	FGF12	fibroblast growth factor 12	2.4	21.3
PBC 002	NXPE3	neurexophilin and PC-esterase domain family member 3	2.4	12.1
PBC 002	MORN4	MORN repeat containing 4	2.3	11.0
PBC 002	RRAS2	related RAS viral (r-ras) oncogene homolog 2	2.3	6.7
PBC 002	AARS	alanyl-tRNA synthetase	2.2	37.5
PBC 002	S100A11	S100 calcium binding protein A11	2.2	4.1
PBC 002	MS4A1	membrane spanning 4-domains A1	2.2	1.0
PBC 002	ZNF593	zinc finger protein 593	2.2	16.6
PBC 002	VPS4B	vacuoloar protein sorting 4 homolog B	2.2	9.0
PBC 002	CHST11	carbohydrate (chondroitin 4) sulfotransferase 11	2.2	15.9
PBC 002	UBXN1	UBX domain protein 1	2.2	2.3
PBC 002	TMEM14C	transmembrane protein 14C	2.2	1.3
PBC 002	NUTM2F	NUT family member 2F	2.2	5.9
PBC 002	TMEM147	transmembrane protein 147	2.2	13.1
PBC 002	ESYT2	extended synaptotagmin protein 2	2.1	37.8
PBC 002	LIPC	lipase C, hepatic type	2.1	2.6
PBC 002	PLBD1	phospholiapse B domain containing 1	2.1	10.6
PBC 002	NLRP5	NLR family, pyrin domain containing 5	2.1	1.2
PBC 002	FN3KRP	fructoamine 3 kinase related protein	2.1	8.7
PBC 002	LINC01558	long intergenic non-protein coding RNA 1558	2.0	7.8
PBC 002	HHEX	hematopoietically expresssed homeobox	2.0	0.9

PBC 002	RRAGD	Ras related GTP binding D	2.0	8.8
PBC 002	NELFE	negative elongation factor complex member E	2.0	16.6
PBC 002	LYPLA1	lysophospholipase I	2.0	3.4
PBC 002	DEFB123	defensin beta 123	2.0	4.8
PBC 002	SRI	sorcin	1.9	1.2
PBC 002	IFI16	interferon, gamma-inducible protein 16	1.9	4.8
PBC 002	ASL	argininosuccinate lyase	1.9	0.8
PBC 002	PPP1R7	protein phosphatase 1 regulatory subunit 7	1.9	3.1
PBC 002	SAYSD1	SAYSVFN motif domain containing 1	1.9	25.3
PBC 002	CA12	carbonic anhydrase XII	1.9	2.4
PBC 002	RAB35	RAB35, member RAS oncogene family	1.9	6.3
PBC 002	TRIM39	tripartite motif containing 39	1.9	10.5
PBC 002	BCKDK	branched chain keotoacid dehydrogenase kinase	1.9	6.2
PBC 002	LAMC2	laminin subunit gamma 2	1.9	1.0
PBC 002	STAC3	SH3 and cysteine rich domain 3	1.9	2.7
PBC 002	SPTLC3	serine palmitoyltransferase long chain base subunit 3	1.9	16.7
PBC 002	PRPSAP1	phosphoribosyl pyrophosphate synthetase-associated protein 1	1.9	1.2
PBC 002	TMEM88	transmembrane protein 88	1.9	5.8
PBC 002	RPA1	replication protein A1	1.9	8.3
PBC 002	TESK1	testis-specific kinase 1	1.8	1.7
PBC 002	PDC-E2	dihydrolipoamide S-acetyltransferase	1.8	3.5
PBC 002	PLCD4	phospholipase C delta 4	1.8	1.5
PBC 002	GPER1	G protein-coupled estrogen receptor 1	1.8	7.6
PBC 002	GIT2	GIT ArfGAP2	1.8	2.2
PBC 002	CADPS	Ca2+ dependent secretion activator	1.8	17.2
PBC 002	FGGY	FGGY carbohydrate kinase domain containing	1.8	9.4
PBC 002	GGH	gamma-glutamyl hydrolase	1.8	14.4
PBC 002	ECHDC3	enoyl-CoA hydratase domain containing 3	1.8	0.9
PBC 002	TSPAN3	tetraspanin 3	1.8	49.5

PBC 002	PRSS36	protease, serine 36	1.8	1.6
PBC 002	EEF1A1	eukaryotic translation elongation factor 1 alpha 1	1.8	8.4
PBC 002	MED8	mediator complex subunit 8	1.8	3.8
PBC 002	DDX50	DEAD-box helicase 50	1.8	7.3
PBC 002	RRAS	related RAS viral (r-ras) oncogene homolog	1.8	7.4
PBC 002	RASL11B	RAS like family 11 member B	1.8	185.9
PBC 002	SCAND2	SCAN domain containing 2	1.8	9.1
PBC 002	SCUBE3	signal peptide, CUB domain and EGF like domain containing 3	1.8	1.9
PBC 002	DUSP22	dual specificity phosphatase 22	1.8	4.3
PBC 002	RNF208	ring finger protein 208	1.8	22.8
PBC 002	CTNNA3	catenin alpha 3	1.8	6.3
PBC 002	TOP1MT	topoisomerase (DNA) I, mitochondrial	1.7	0.9
PBC 002	GDF6	growth differentiation factor 6	1.7	3.5
PBC 002	KCNF1	potassium voltage-gated channel modifier subfamily member 1	1.7	8.5
PBC 002	NKAP	NFKB activating protein	1.7	10.3
PBC 002	C1orf43	chromosome 1 open reading frame 43	1.7	6.0
PBC 002	STRADB	STE20-related kinase adaptor beta	1.7	4.9
PBC 002	SOD1	superoxide dismutase 1, soluble	1.7	1.6
PBC 002	EGFL7	EGF like domain multiple 7	1.7	17.1
PBC 002	SERPINA10	serpin peptidase inhibitor, clade A	1.7	8.0
PBC 002	HAP1	huntingtin-associated protein 1	1.7	3.8
PBC 002	SH3YL1	SH3 and SYLF domain containing 1	1.7	8.2
PBC 002	DECR2	2,4-dienoyl-CoA reductase 2, peroxisomal	1.7	1.8
PBC 002	ACSM5	acyl-CoA synthetase medium-chain family member 5	1.7	16.0
PBC 002	TMEM187	transmembrane protein 187	1.7	7.1
PBC 002	PRAMEF22	PRAME family member 22	1.7	4.7
PBC 002	DIRAS3	DIRAS family GTP binding RAS like 3	1.7	2.0
PBC 002	FGF20	fibroblast growth factor 20	1.7	0.6

PBC 002	ZNF227	zinc finger protein 227	1.7	2.0
PBC 002	WFIKKN1	WAP, follistatin/kazal, immunoglobulin, kunitz and netrin domain containing 1	1.7	8.5
PBC 002	ZNF517	zinc finger protein 517	1.7	12.0
PBC 002	BIN3-IT1	BIN3 intronic transcript 1	1.7	6.4
PBC 002	JTB	jumping translocation breakpoint	1.7	3.2
PBC 002	PGS1	phosphatidylglycerophosphate synthase	1.7	6.0
PBC 002	EIF3S2	eukaryotic translation initiation factor 3 subunit I	1.7	1.8
PBC 002	BMP15	bone morphogenetic protein 15	1.6	3.0
PBC 002	TNK1	tyrosine kinase, non-receptor, 1	1.6	21.5
PBC 002	RASD2	RASD family member 2	1.6	9.5
PBC 002	SULF2	sulfatase 2	1.6	7.0
PBC 002	DSTNP4	destrin (actin depolymerizing factor) pseudogene 4	1.6	1.2
PBC 002	TXN2	thioredoxin 2	1.6	116.0
PBC 002	SIGLEC10	sialic acid binding Ig like lectin 10	1.6	1.1
PBC 002	MEOX2	mesenchyme homeobox 2	1.6	24.4
PBC 002	RELT	RELT tumor necrosis factor receptor	1.6	16.1
PBC 002	C21orf91	chromosome 21 open reading frame 91	1.6	5.4
PBC 002	PXYLP1	2-phosphoxylose phosphatase 1	1.6	2.9
PBC 002	CMBL	carboxymethylenebutenolidase homolog	1.6	0.8
PBC 002	TEKT4	tektin 4	1.6	3.8
PBC 002	ATP5O	ATP synthase, H+ transporting, mitochondrial F1 complex, O subunit	1.6	1.8
PBC 002	PPBP	pro-platelet basic protein	1.6	4.8
PBC 002	PAPPA2	pappalysin 2	1.6	4.2
PBC 002	CHRNA3	cholinergic receptor nicotinic alpha 3 subunit	1.6	8.4
PBC 002	PSAPL1	prosaposin-like 1	1.6	23.1
PBC 002	ALKBH8	alkB homolog 8, tRNA methyltransferase	1.6	6.0
PBC 002	CAPN1	calpain 1	1.6	103.2
PBC 002	RPH3AL	rabphilin 3A-like	1.6	3.1
PBC 002	EBP	emopamil binding protein	1.6	19.4

PBC 002	FH	fumarate hydratase	1.6	0.9
PBC 002	KCNIP3	potassium voltage-gated channel interacting protein 3	1.6	1.4
PBC 002	MTCP1	mature T-cell proliferation 1	1.6	3.6
PBC 002	ATP5SL	ATP5S-like	1.6	2.0
PBC 002	CXCL3	C-X-C motif chemokine ligand 3	1.6	21.1
PBC 002	KCNS3	potassium voltage-gated channel modifier subfamily S member 3	1.6	5.2
PBC 002	STMN3	stathmin 3	1.6	10.4
PBC 002	IPPK	inositol-pentakisphosphate 2-kinase	1.6	25.8
PBC 002	MTBP	MDM2 binding protein	1.6	4.5
PBC 002	SLC30A3	solute carrier family 30 member 3	1.6	1.3
PBC 002	CENPBD1	CENPB DNA-binding domain containing 1	1.6	6.1
PBC 002	RTKN	rhotekin	1.6	6.6
PBC 002	AIDA	axin interactor, dorsalization associated	1.6	4.2
PBC 002	USP53	ubiquitin specific peptidase 53	1.6	12.6
PBC 002	ZP1	zona pellucida glycoprotein 1	1.6	5.8
PBC 002	KIAA0368	KIAA0368	1.6	8.3
PBC 002	DCLRE1C	DNA cross-link repair 1C	1.6	7.7
PBC 002	LALBA	lactalbumin alpha	1.6	4.1
PBC 002	EMX2	empty spiracles homeobox 2	1.6	17.1
PBC 002	HLA-E	major histocompatibility complex, class I, E	1.6	7.3
PBC 002	RTN4	reticulon 4	1.6	7.6
PBC 002	ANGPTL3	angiopoietin like 3	1.5	7.4
PBC 002	GP2	glycoprotein 2	1.5	1.0
PBC 002	BTN2A2	butyrophilin subfamily 2 member A2	1.5	0.7
PBC 002	GPR82	G protein-coupled receptor 82	1.5	27.1
PBC 002	SHISA3	shisa family member 3	1.5	7.5
PBC 002	TMED6	transmembrane p24 trafficking protein 6	1.5	5.6
PBC 002	TBC1D15	TBC1 domain family member 15	1.5	5.0
PBC 002	ZBTB9	zinc finger and BTB domain containing 9	1.5	6.6

PBC 002	GGT2	gamma-glutamyltransferase 2	1.5	4.8
PBC 002	CD40	CD40 molecule	1.5	5.5
PBC 002	TARS2	threonyl-tRNA synthetase 2, mitochondrial	1.5	14.5
PBC 002	NTN4	netrin 4	1.5	1.3
PBC 002	MATN3	matrilin 3	1.5	0.6
PBC 002	LINC01547	long intergenic non-protein coding RNA 1547	1.5	3.6
PBC 002	CNOT2	CCR4-NOT transcription complex subunit 2	1.5	17.1
PBC 002	NMT2	N-myristoyltransferase 2	1.5	6.2
PBC 002	RSPO4	R-spondin 4	1.5	17.9
PBC 002	PRPS1	phosphoribosyl pyrophosphate synthetase 1	1.5	5.1
PBC 002	SDF4	stromal cell derived factor 4	1.5	1.7
PBC 002	HLA-DMA	major histocompatibility complex, class II, DM alpha	1.5	26.7
PBC 002	GPN3	GPN-loop GTPase 3	1.5	1.0
PBC 002	PHF10	PHD finger protein 10	1.5	11.5
PBC 002	WRAP73	WD repeat containing, antisense to TP73	1.5	0.5
PBC 002	SMCP	sperm mitochondria associated cysteine rich protein	1.5	1.6
PBC 002	NPSR1	neuropeptide S receptor 1	1.5	4.4
PBC 002	C1QTNF8	C1q and tumor necrosis factor related protein 8	1.5	1.3
PBC 002	TNFRSF21	tumor necrosis factor receptor superfamily member 21	1.5	2.1
PBC 002	CDK16	cyclin-dependent kinase 16	1.5	18.2
PBC 002	PTCRA	pre T-cell antigen receptor alpha	1.5	7.9
PBC 002	CFAP45	cilia and flagella associated protein 45	1.5	12.0
PBC 002	LBX2-AS1	LBX2 antisense RNA 1	1.5	10.3
PBC 002	NOSTRIN	nitric oxide synthase trafficking	1.5	1.7
PBC 002	ARL8A	ADP ribosylation factor like GTPase 8A	1.5	1.6
PBC 002	FAM83F	family with sequence similarity 83 member F	1.5	6.6
PBC 002	MORC1	MORC family CW-type zinc finger 1	1.5	5.9
PBC 002	PLD4	phospholipase D family member 4	1.5	4.8
PBC 002	DLL1	delta-like 1	1.5	4.2
PBC 002	LTB4R	leukotriene B4 receptor	1.5	5.3

PBC 002	ARL4D	ADP ribosylation factor like GTPase 4D	1.5	38.0
PBC 002	PDK1	pyruvate dehydrogenase kinase 1	1.5	0.5
PBC 002	MAPK1	mitogen-activated protein kinase 1	1.5	1.1
PBC 002	JPH3	junctophilin 3	1.5	11.6
PBC 002	SFTPA1	surfactant protein A1	1.5	7.8
PBC 002	CCDC173	coiled-coil domain containing 173	1.5	1.9
PBC 002	CAPN2	calpain 2	1.5	0.6
PBC 002	MORN1	MORN repeat containing 1	1.5	10.6
PBC 002	SERPINA1 1	serpin peptidase inhibitor, clade A (alpha-1 antiproteinase, antitrypsin), member 11	1.5	16.7
PBC 002	DUSP8	dual specificity phosphatase 8	1.5	4.9
PBC 002	BTBD2	BTB domain containing 2	1.5	3.2
PBC 002	MINK1	misshapen-like kinase 1	1.5	9.7
PBC 002	RGS13	regulator of G-protein signaling 13	1.5	84.3
PBC 002	RPL10L	ribosomal protein L10 like	1.5	17.5
PBC 002	PSTK	phosphoseryl-tRNA kinase	1.5	20.8
PBC 002	RPL18	ribosomal protein L18	1.5	2.0
PBC 002	CFP	complement factor properdin	1.5	6.2
PBC 002	MLLT10	myeloid/lymphoid or mixed-lineage leukemia; translocated to, 10	1.5	1.3

Sample	**Target**	**Gene name**	**Z-score**	**IS**
PBC 003	HK1	hexokinase 1	20.7	3.6
PBC 003	NXN	nucleoredoxin	10.5	1.9
PBC 003	GPD1	glycerol-3-phosphate dehydrogenase 1	8.4	1.4
PBC 003	SPRR1A	small proline rich protein 1A	7.8	1.3
PBC 003	SPRR3	small proline rich protein 3	6.3	1.1
PBC 003	ECE2	endothelin converting enzyme 2	5.4	0.9
PBC 003	PPP1R11	protein phosphatase 1 regulatory inhibitor subunit 11	4.6	0.8
PBC 003	CUTA	cutA divalent cation tolerance homolog (E. coli)	4.1	0.7

PBC 003	SULT2A1	sulfotransferase family 2A member 1	3.7	0.6
PBC 003	TMOD1	tropomodulin 1	3.6	0.6
PBC 003	DIABLO	diablo, IAP-binding mitochondrial protein	3.6	0.6
PBC 003	APITD1	apoptosis-inducing, TAF9-like domain 1	3.6	0.6
PBC 003	CTBP1	C-terminal binding protein 1	3.3	0.6
PBC 003	NGB	neuroglobin	2.9	0.5
PBC 003	GATSL2	GATS protein-like 2	2.7	0.5
PBC 003	KRTAP17-1	keratin associated protein 17-1	2.6	0.5
PBC 003	FOXA3	forkhead box A3	2.6	1.5
PBC 003	PDHB	pyruvate dehydrogenase (lipoamide) beta	2.4	1.6
PBC 003	RAB11A	RAB11A, member RAS oncogene family	2.4	0.4
PBC 003	ITM2C	integral membrane protein 2C	2.3	33.3
PBC 003	PQBP1	polyglutamine binding protein 1	2.2	0.4
PBC 003	GGA1	golgi-associated, gamma adaptin ear containing, ARF binding protein 1	2.1	0.4
PBC 003	RLBP1	retinaldehyde binding protein 1	2.0	0.3
PBC 003	ZNF696	zinc finger protein 696	2.0	0.4
PBC 003	PSMA4	proteasome subunit alpha 4	1.9	0.3
PBC 003	CDKN2C	cyclin-dependent kinase inhibitor 2C	1.9	0.3
PBC 003	DNAJC12	DnaJ heat shock protein family (Hsp40) member C12	1.8	0.3
PBC 003	BEX5	brain expressed X-linked 5	1.8	0.3
PBC 003	BCL2L11	BCL2 like 11	1.8	0.3
PBC 003	MAPK1IP1L	mitogen-activated protein kinase 1 interacting protein 1-like	1.6	0.3
PBC 003	PSMB6	proteasome subunit beta 6	1.6	0.3
PBC 003	PDC-E2	dihydrolipoamide S-acetyltransferase	1.5	3.7

SUPPLEMENTARY MATERIAL – TABLE 2

		Immunostaining for nucleolar protein 3 (NOL3)		
Sample	**NOL3 antibodies**	**lymphocytes**	**cholangiocytes**	**hepatocytes**
PSC 1	–	occasional	++ / +++	+
PSC 2	–	occasional	++	+
PSC 3	–	occasional	++ / +++	+ / ++
PSC 4	+	occasional	++	+
PSC 5	–	negative	+ / ++	+
PSC 6	+	occasional	++ / +++	+ / ++
PSC 7	+	positive	++ / +++	+ / ++
PSC 8	+	positive	++	+
PSC 9	+	positive	++	+
PBC 1	–	negative	+ / ++	+
PBC 2	–	occasional	+	+
PBC 3	–	occasional	+	+

SUPPLEMENTARY MATERIAL – FIGURE 1

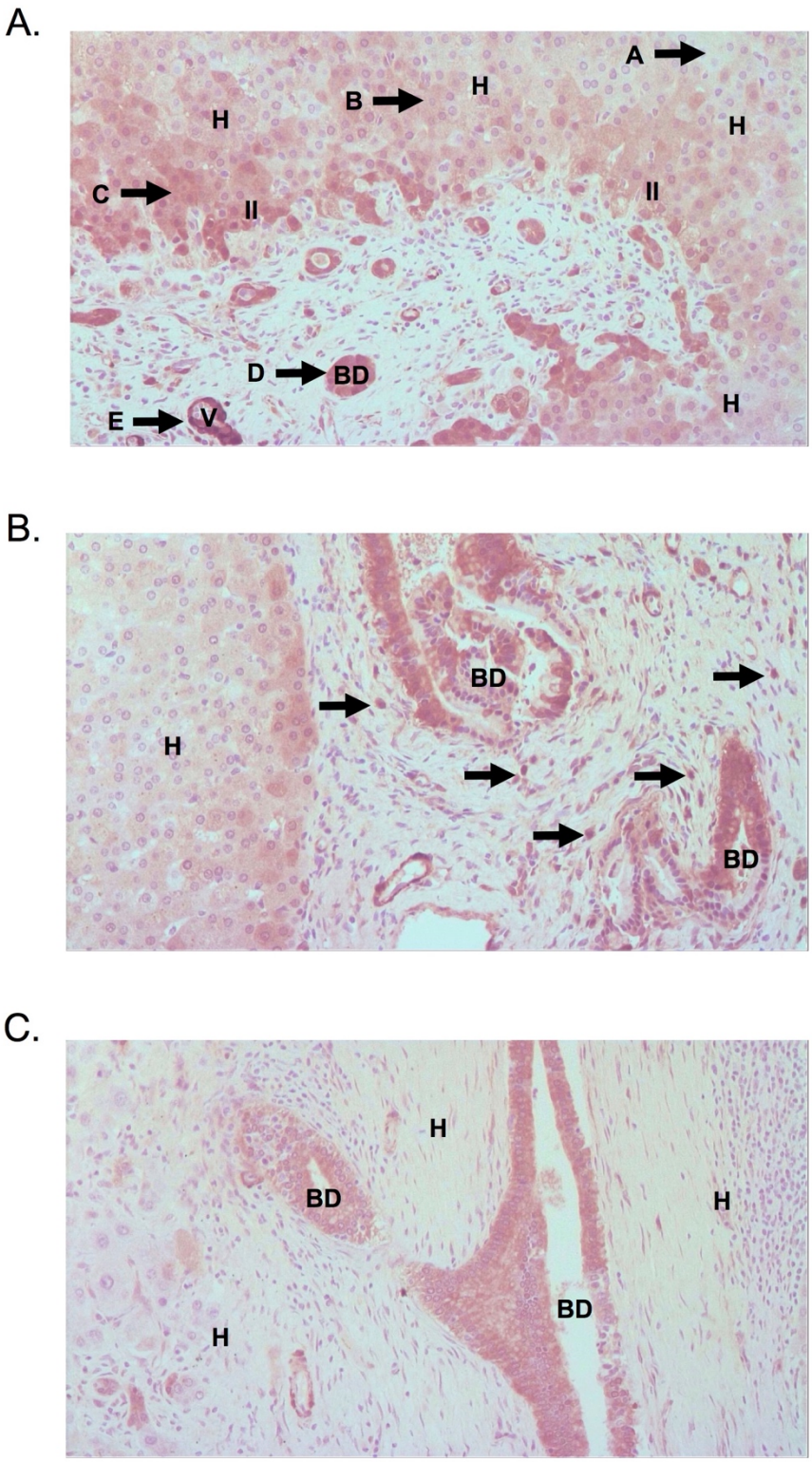

D.

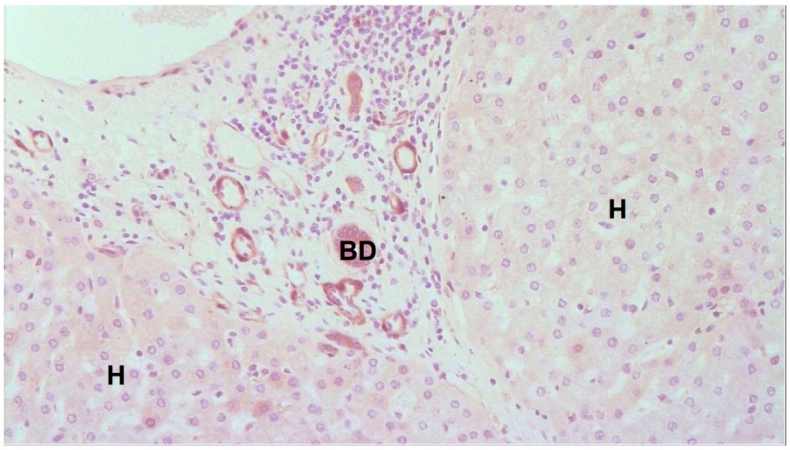

SUPPLEMENTARY MATERIAL – FIGURE 2

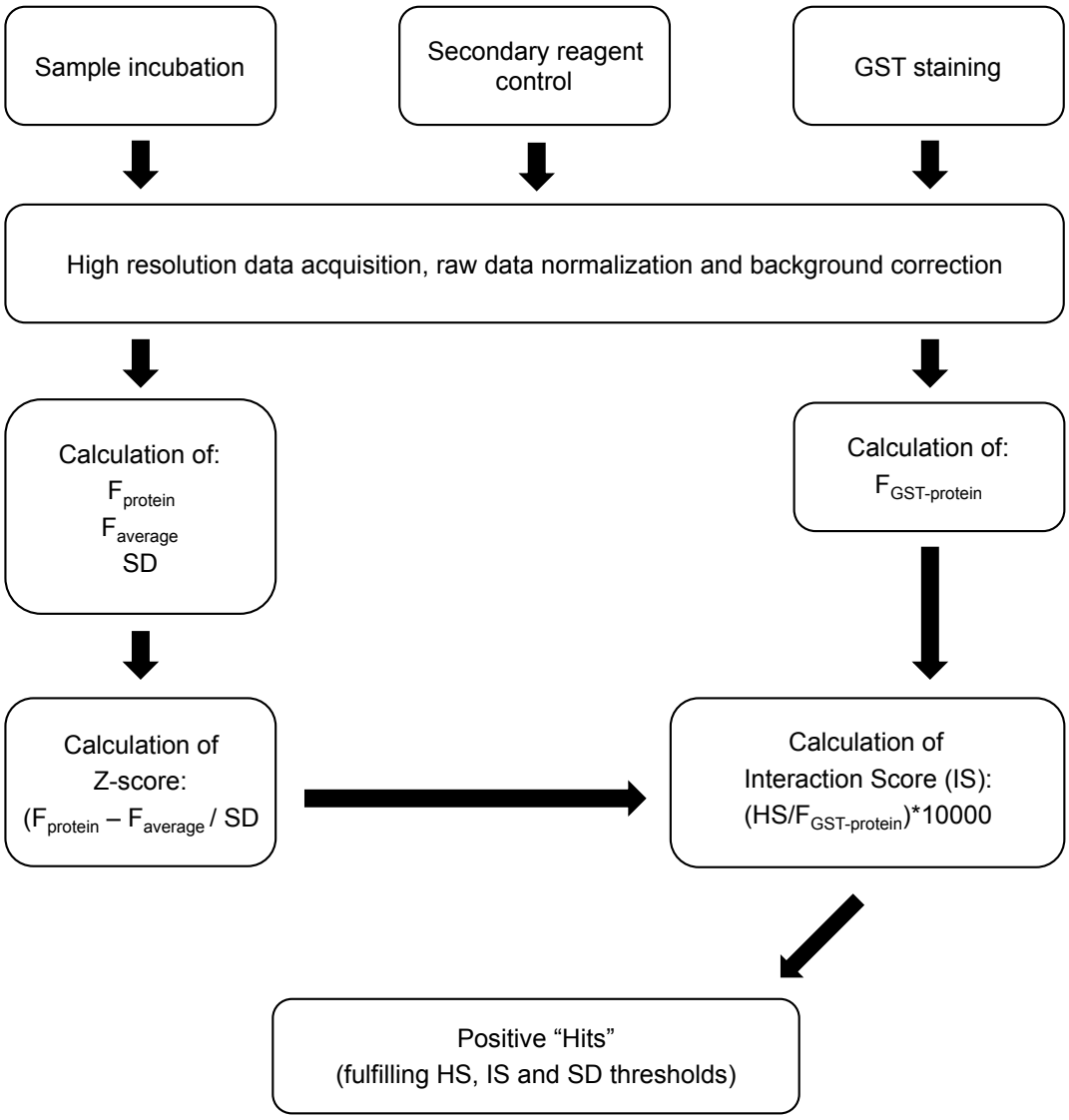

SUPPLEMENTARY MATERIAL – FIGURE 3

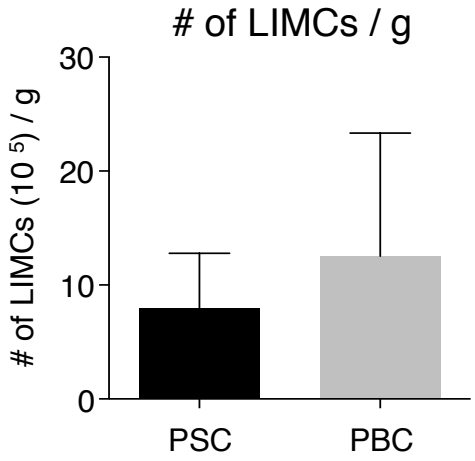
# of LIMCs / g
# of LIMCs (10 5) / g
30
20
10
0
PSC
PBC

SUPPLEMENTARY MATERIAL – FIGURE 4

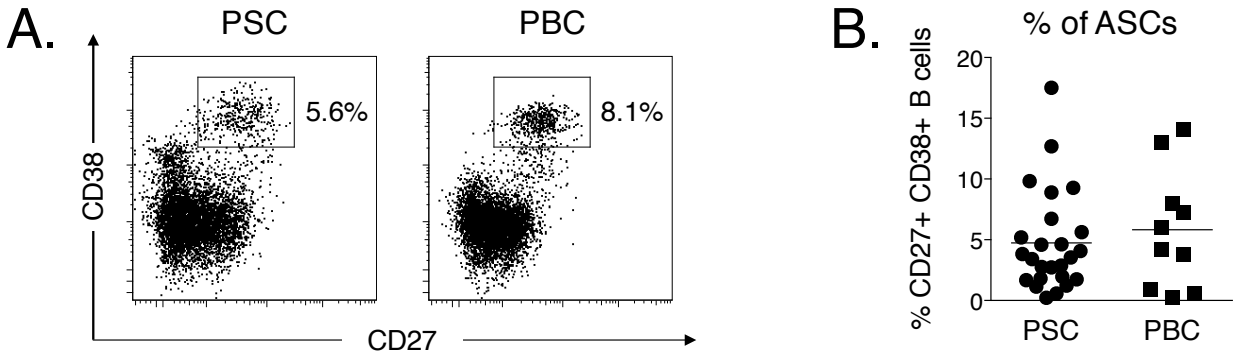

SUPPLEMENTARY MATERIAL – FIGURE 5

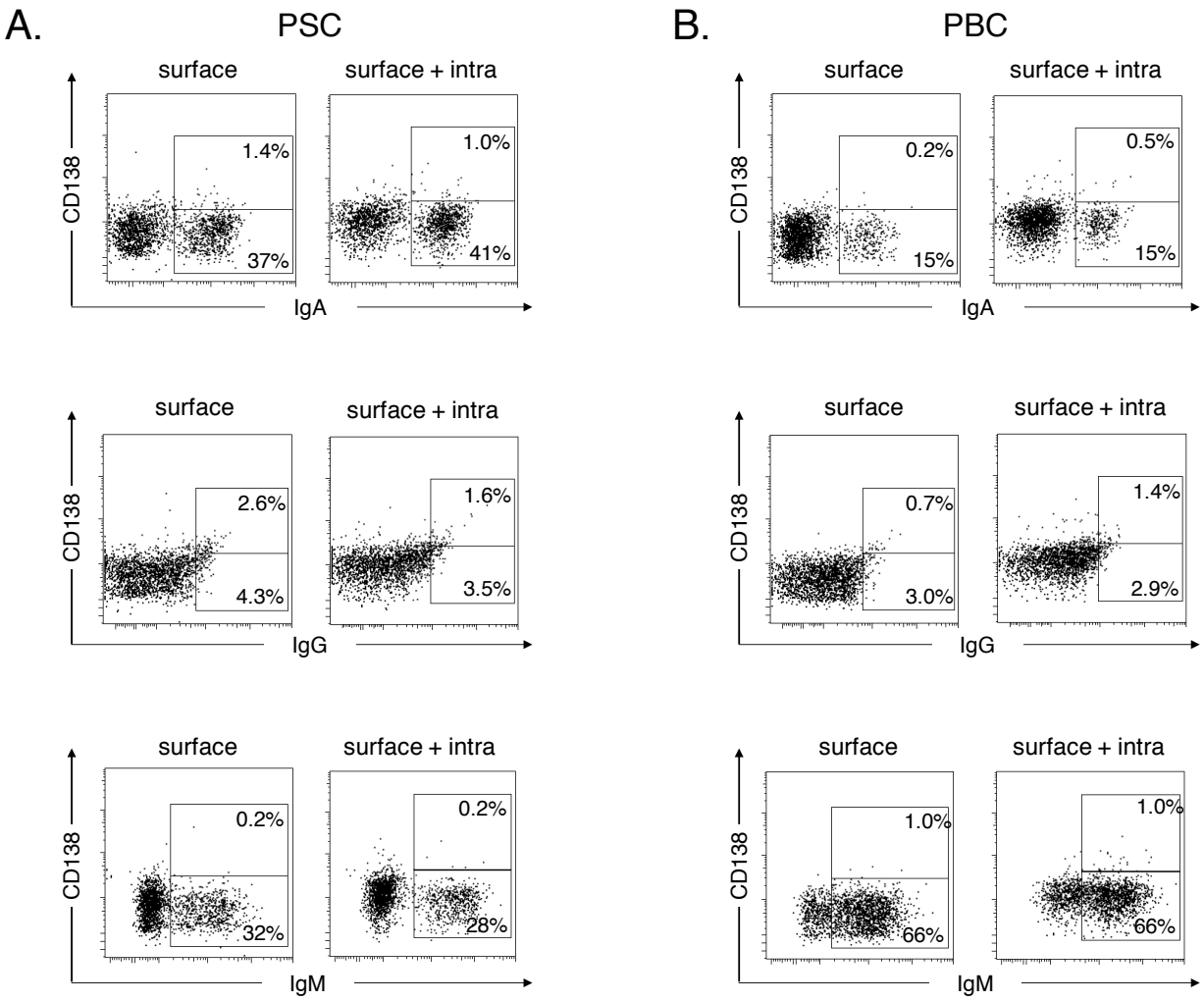

SUPPLEMENTARY MATERIAL – FIGURE 6

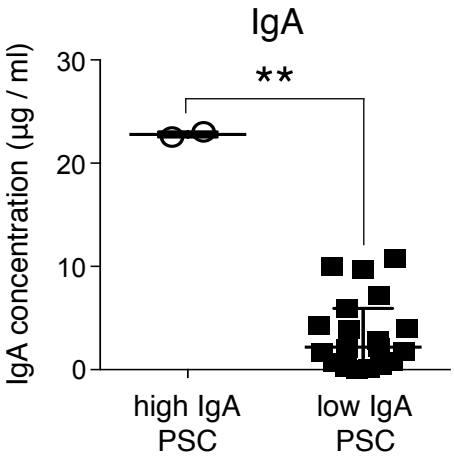

SUPPLEMENTARY MATERIAL – FIGURE 7

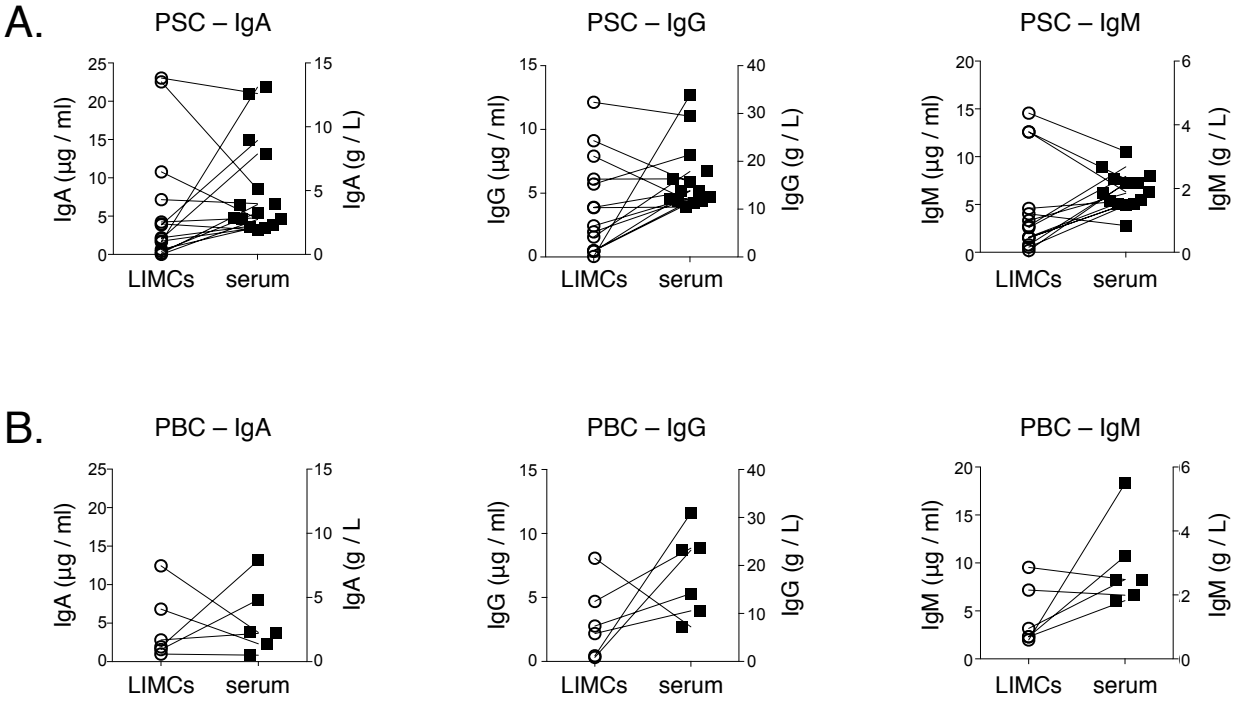

SUPPLEMENTARY MATERIAL – FIGURE 8